Interaction between MED12 and ΔNp63 activates basal identity in pancreatic ductal adenocarcinoma

Diogo Maia-Silva[1], Patrick J. Cunniff [1], Allison C. Schier[2], Damianos Skopelitis[1], Marygrace C. Trousdell [1], Philip Moresco [1], Yuan Gao [1], Vahag Kechejian[1], Xue-Yan He [1], Yunus Sahin [1], Ledong Wan [1], Aktan Alpsoy [1], Jynelle Liverpool[1], Adrian R. Krainer [1], Mikala Egeblad[1], David L. Spector [1], Douglas T. Fearon[1], Camila O. dos Santos [1], Dylan J. Taatjes[2] & Christopher R. Vakoc [1] ✉

The presence of basal lineage characteristics signifies hyperaggressive human adenocarcinomas of the breast, bladder and pancreas. However, the biochemical mechanisms that maintain this aberrant cell state are poorly understood. Here we performed marker-based genetic screens in search of factors needed to maintain basal identity in pancreatic ductal adenocarcinoma (PDAC). This approach revealed MED12 as a powerful regulator of the basal cell state in this disease. Using biochemical reconstitution and epigenomics, we show that MED12 carries out this function by bridging the transcription factor ΔNp63, a known master regulator of the basal lineage, with the Mediator complex to activate lineage-specific enhancer elements. Consistent with this finding, the growth of basal-like PDAC is hypersensitive to MED12 loss when compared to PDAC cells lacking basal characteristics. Taken together, our genetic screens have revealed a biochemical interaction that sustains basal identity in human cancer, which could serve as a target for tumor lineage-directed therapeutics.

Cellular identity is commonly dysregulated in human cancer[1]. As a prominent example, human adenocarcinomas, which are tumors of the glandular epithelial lineage, can acquire characteristics of basal (also known as squamous) epithelial cells during disease progression[2]. This process is most evident in poor prognosis adenocarcinomas of the breast[3,4], bladder[5,6] and pancreas[7–10]; tumors that express basal lineage markers (for example, TP63 and KRT5), which are normally restricted to squamous cell carcinomas. Emerging evidence in human lung adenocarcinoma also highlights the acquisition of basal characteristics as a means of bypassing EGFR[11] or KRAS[12]-targeting therapeutics. While the clinical significance of basal-like adenocarcinomas has become clear

in recent years, the biochemical mechanisms that drive this aberrant cell fate remain largely unknown.

One critical master regulator of the basal lineage in normal[13] and neoplastic contexts[14] is the transcription factor p63 (ΔN isoform), the protein product of the TP63 gene. While largely undetectable in the normal human and mouse pancreas[15,16], a subset of pancreatic ductal adenocarcinomas (PDAC) acquires ΔNp63 expression in close association with a basal-like transcriptome and inferior patient outcomes[9,10,17–19]. We and others previously demonstrated the necessity and sufficiency of ΔNp63 to endow PDAC cells with basal lineage characteristics[18,20], which in turn leads to enhanced cell motility and invasion[18],

[1]Cold Spring Harbor Laboratory, Cold Spring Harbor, NY, USA. [2]Department of Biochemistry, University of Colorado, Boulder, CO, USA. ✉e-mail: vakoc@cshl.edu
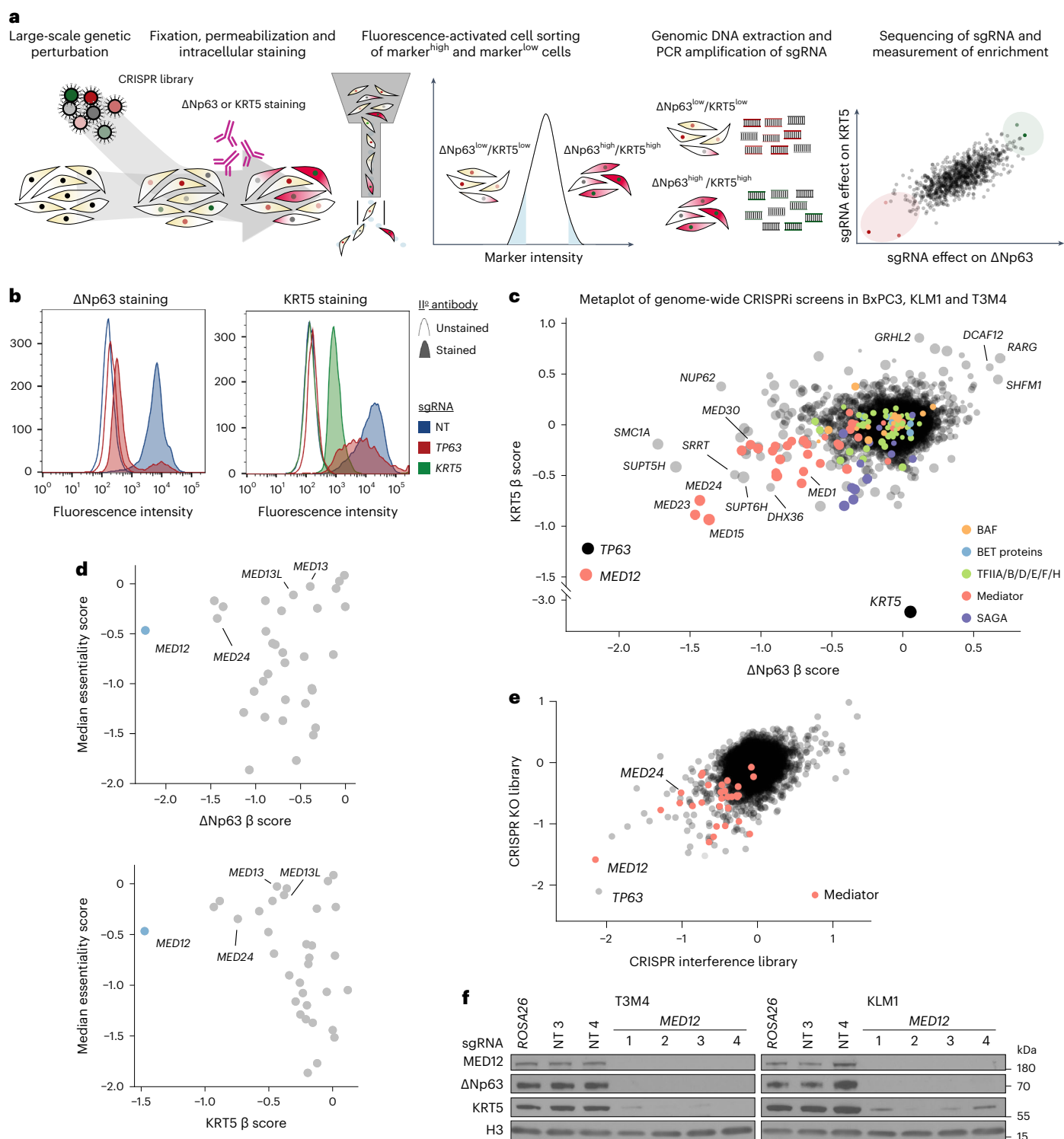
Fig. 1 | Intracellular FACS-based genome-wide CRISPR screens uncover *MED12* as a critical regulator of basal lineage identity in PDAC. a, Diagram illustrating the workflow of KRT5 or ΔNp63 genome-wide reporter screens. **b**, Representative flow cytometry staining profiles for CRISPRi-mediated *TP63* or *KRT5* knockdown in KLM1 cells. Secondary staining with AF647-conjugated anti-rabbit antibody (area-filled curves) or unstained controls (outline-only curves) show the signal distribution of (left) ΔNp63- or (right) KRT5-stained cells upon gene knockdown. A minimum of 10,000 events were collected and plotted for each sample. **c**, Metaplot of ΔNp63- and KRT5-based reporter genome-wide CRISPRi screen results in three independent cell lines (KLM1, T3M4 and BxPC3). Average β scores of ΔNp63 and KRT5 screens are plotted such that each dot represents one promoter-defined gene. The size of each dot is proportional to the inverse

of the s.d. of the β values across cell lines. Important mammalian general transcriptional regulators are highlighted according to the legend. β scores were calculated using MAGeCK with the maximum likelihood estimation option, with negative β scores denoting enrichment in the marker^low population. **d**, Scatterplot of the average β scores in the ΔNp63 (top) or KRT5 (bottom) reporter screens across KLM1, T3M4 and BxPC3, and the median CERES cancer cell line essentiality scores from the cancer dependency map. **e**, Scatterplot of ΔNp63-based reporter screens β scores using genome-wide CRISPRi or CRISPR knockout libraries in KLM1 cells. Genes belonging to the Mediator complex are highlighted in red. **f**, Western blot of whole cell lysates at day 6 post-infection with lentiviral CRISPR knockout sgRNA targeting *MED12* or negative control sgRNAs in T3M4 and KLM1 cells.

stromal inflammation[21], chemotherapy resistance[22] and a powerful ΔNp63 dependency for cell viability and proliferation[18,21,23]. Despite this potent transcriptional activation function seen in vivo, ΔNp63 lacks a critical N-terminal activation domain present on the full-length protein[9,18]. The biochemical mechanism by which ΔNp63 activates basal identity in PDAC has yet to be defined.

The Mediator complex is a multisubunit transcriptional coactivator required for most RNA polymerase II-dependent transcription in eukaryotes[24]. This general transcriptional role depends on the core Mediator, which is composed of 26 subunits that lack any known enzymatic activity. However, a reversibly attached four-subunit Mediator kinase module (MKM), comprised of MED12 or MED12L, MED13 or MED13L, cyclin C and CDK8 or CDK19, contributes to transcription through phosphorylation of protein substrates[25]. Unlike the broad requirements for core Mediator in transcription, the MKM performs specialized transcriptional functions in a context-specific manner[25–27].

To complement prior hypothesis-oriented studies of basal-like PDAC[18,20], we set out to develop a marker-based CRISPR screening method capable of revealing all genes needed to maintain basal identity in this disease (Fig. 1a). Our approach relies on intracellular fluorescent-activated cell sorting (FACS) staining of ΔNp63 and KRT5, which are validated diagnostic markers that distinguish basal-like tumors from classical adenocarcinomas[9,17,24,28–30]. After optimizing the staining conditions and the quantitative resolution of the assay (Fig. 1b and Extended Data Fig. 1a), we performed genome-wide CRISPR interference (CRISPRi) screens[31] in three basal-like PDAC cell line models (T3M4, KLM1 and BxPC3)[18,20,21,32], measuring the effects of >20,000 genetic perturbations on KRT5 and ΔNp63 expression (Fig. 1c and Supplementary Table 1). These models were chosen because they best resemble the transcriptome of basal-like PDAC tumors, including high-level expression of ΔNp63/KRT5 (Supplementary Table 2). In all six screens, the outlier performance of KRT5 and TP63 single guide RNAs (sgRNAs) supported the overall quality of these datasets (Fig. 1c). Because ΔNp63 directly activates KRT5 (Extended Data Fig. 1b) and its own expression at the TP63 locus[33,34], we reasoned that any additional outlier hits identified across these screens might represent factors that cooperate biochemically with ΔNp63 to activate basal lineage features.

All six of our genetic screens independently nominated MED12 as encoding a top genetic requirement for ΔNp63 and KRT5 expression in basal-like PDAC (Supplementary Table 1). Notably, the MED12 requirement for ΔNp63 and KRT5 expression exceeded that of all other Mediator subunits and other general transcriptional machineries (for example, TFIID, p300, BAF complex and BET proteins; Fig. 1c). While most of the core subunits of Mediator are pan-essential dependencies across all cancer cell lines, MED12 exhibits cell line selectivity in its essentiality requirement (Fig. 1d). To validate our results, we repeated our marker-based screen using a genome-wide CRISPR knockout sgRNA

library[35], which also recovered TP63 and MED12 as outlier requirements for basal lineage identity (Fig. 1e). We cloned and tested individual sgRNAs targeting MED12, and validated potent downregulation of MED12, ΔNp63 and KRT5 at the protein level via western blotting analysis in three different basal-like PDAC models (Fig. 1f and Extended Data Fig. 1c). In addition, we found MED12 to be required for ΔNp63 and KRT5 expression in basal-like triple-negative breast cancer (Extended Data Fig. 1d,e) and in cell line models of squamous cell carcinoma of the skin, head and neck and esophagus (Extended Data Fig. 1d). Collectively, our screening results provided a strong rationale to investigate MED12 as a regulator of basal identity in PDAC.

We next performed RNA sequencing (RNA-seq) analysis following CRISPR-based targeting of MED12 and TP63 in T3M4 and KLM1 cells, which led to a broad suppression of clinically-defined basal lineage signatures[10] (Fig. 2a,b, Extended Data Fig. 2a and Supplementary Table 3). MED12 knockout (KO) also substantially suppressed a core set of previously defined[18] direct ΔNp63 target genes in PDAC (Fig. 2b and Extended Data Fig. 2a) and non-PDAC basal/squamous carcinoma models (Extended Data Fig. 2b and Supplementary Table 4). As a control for specificity, knockout of other essential genes (for example, CDK1, SUPT20H and PCNA) failed to suppress basal and ΔNp63 target gene signatures (Fig. 2a and Supplementary Table 3). To extend these findings, we performed single-cell RNA-seq of BxPC3, T3M4 and the human basal-like PDAC organoid hF3 (ref. 36). In all three models, both TP63 and MED12 knockout led to suppression of a basal-like gene signature (Extended Data Fig. 2c,d). Additionally, while TP63 knockout caused the upregulation of a classical gene signature, loss of MED12 led instead to activation of an interferon response. This is consistent with the known role of MED12 as an antagonist of STAT transcription factors[27] (Extended Data Fig. 2c,d). We next sought to distinguish whether MED12 directly activates the basal lineage transcriptome or indirectly supports basal identity by simply activating TP63 transcription. Results from RT-qPCR timecourse measurements indicated that KRT5 and TP63 become downregulated with similar kinetics following MED12 inactivation (Fig. 2c and Extended Data Fig. 2e). In addition, constitutive lentiviral expression of a ΔNp63 complementary DNA (cDNA) failed to rescue the MED12 requirement for the expression of basal lineage genes (Fig. 2d). These findings suggest that ΔNp63 and MED12 are each required to activate the basal lineage transcriptional signature in PDAC.

We next performed ChIP–seq analysis of ΔNp63 and MED12 localization across the genome of basal-like PDAC models. Chromatin occupancy profiling of ΔNp63 and MED12 revealed significant overlap in both KLM1 and T3M4 cells at active cis-regulatory elements enriched for H3K27 acetylation (Fig. 2e and Extended Data Fig. 3a). This pattern of shared occupancy included a class of 'basal lineage enhancers' that we defined previously as selectively activated in basal-like PDAC models[18]. We hypothesized that ΔNp63, as a sequence-specific DNA-binding protein, was responsible for tethering MED12 to these

**Fig. 2 | ΔNp63 recruits MED12 to chromatin to co-activate the basal transcriptional signature. a**, Heatmap of z-scored variance-stabilizing transformed gene counts of top 250 overexpressed and downregulated genes upon TP63 knockout in T3M4 cells. Columns correspond to individual knockout RNA-seq samples (n = 3 biological replicates per sgRNA). Samples are clustered using Euclidean distance. Genes associated with basal (right) and classical (left) PDAC are labeled. **b**, Representative GSEA plots of T3M4 MED12 knockout using gene signatures derived from human basal PDAC tumors[10] and direct ΔNp63 gene targets in PDAC[18]. NES, normalized enrichment score. GSEA for all sgRNA and cell lines tested can be found in Supplementary Table 3. **c**, Timecourse RT-qPCR of TP63 and its target gene KRT5 after CRISPRi knockdown of TP63, MED12 or controls in T3M4 cells. −ΔΔCt values are plotted as the average of all sgRNA targeting each gene normalized to the average of ACTB and B2M (three measurements per condition). Average −ΔΔCt of independent sgRNA is shown as solid lines and the respective 95% confidence intervals are shown as translucid intervals. **d**, RT-qPCR of TP63 and its target genes S100A2, IL1B and KRT6A after

ΔNp63 overexpression and MED12 CRISPRi knockdown. Messenger RNA (mRNA) fold change values are calculated as $2^{-\Delta\Delta Ct}$ normalized to the average of ACTB, B2M and PPIA. Dots represent the average of three measurements per sgRNA, and bars represent the mean of two independent measurements. Double-sided t test P values are shown in the figure. **e**, Metaplots and heatmaps of ΔNp63, MED12 and acetylated H3K27 (H3K27ac) chromatin occupancy in KLM1 cells. Signal intensity values are centered around and sorted by ΔNp63 peak intensity. **f**, Metaplots of ΔNp63 (left) and MED12 (right) genome occupancy centered around MED12 peaks at basal enhancers in KLM1 cells upon ROSA26 or TP63 knockout (two different sgRNAs). **g**, ChIP–seq tracks of ΔNp63, MED12 and H3K27ac normalized occupancy at select basal-specific ΔNp63 direct target loci in KLM1 cells upon ROSA26 or TP63 knockout. One additional TP63 knockout sgRNA is shown in Extended Data Fig. 3b. **h**, Metaplots of ΔNp63 (left) and MED12 (right) genome occupancy centered around MED12-occupied peaks neighboring ΔNp63 direct target genes in SUIT2 CRISPRa-TP63 lines. **e,f,h**, One independent measurement per condition is shown.

basal enhancer elements. In support of this, genetic inactivation of ΔNp63 led to severe reductions in MED12 occupancy at basal lineage enhancers (Fig. 2f,g, Extended Data Fig. 3b and Supplementary

Table 5). In the converse experiment, we found that ectopic expression of ΔNp63 in a classical PDAC model was sufficient to acquire MED12 occupancy at core ΔNp63 targets in PDAC (Fig. 2h, Extended Data
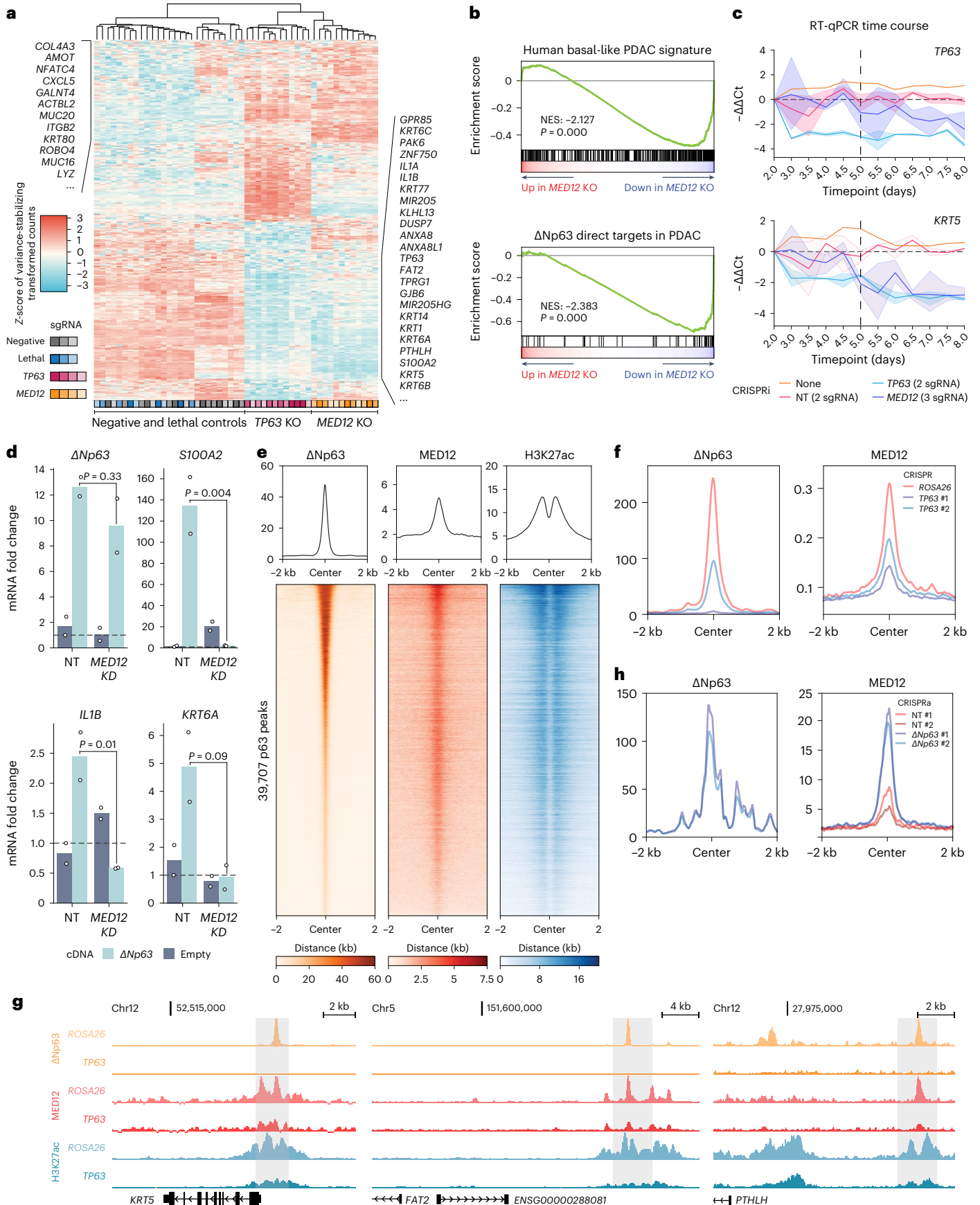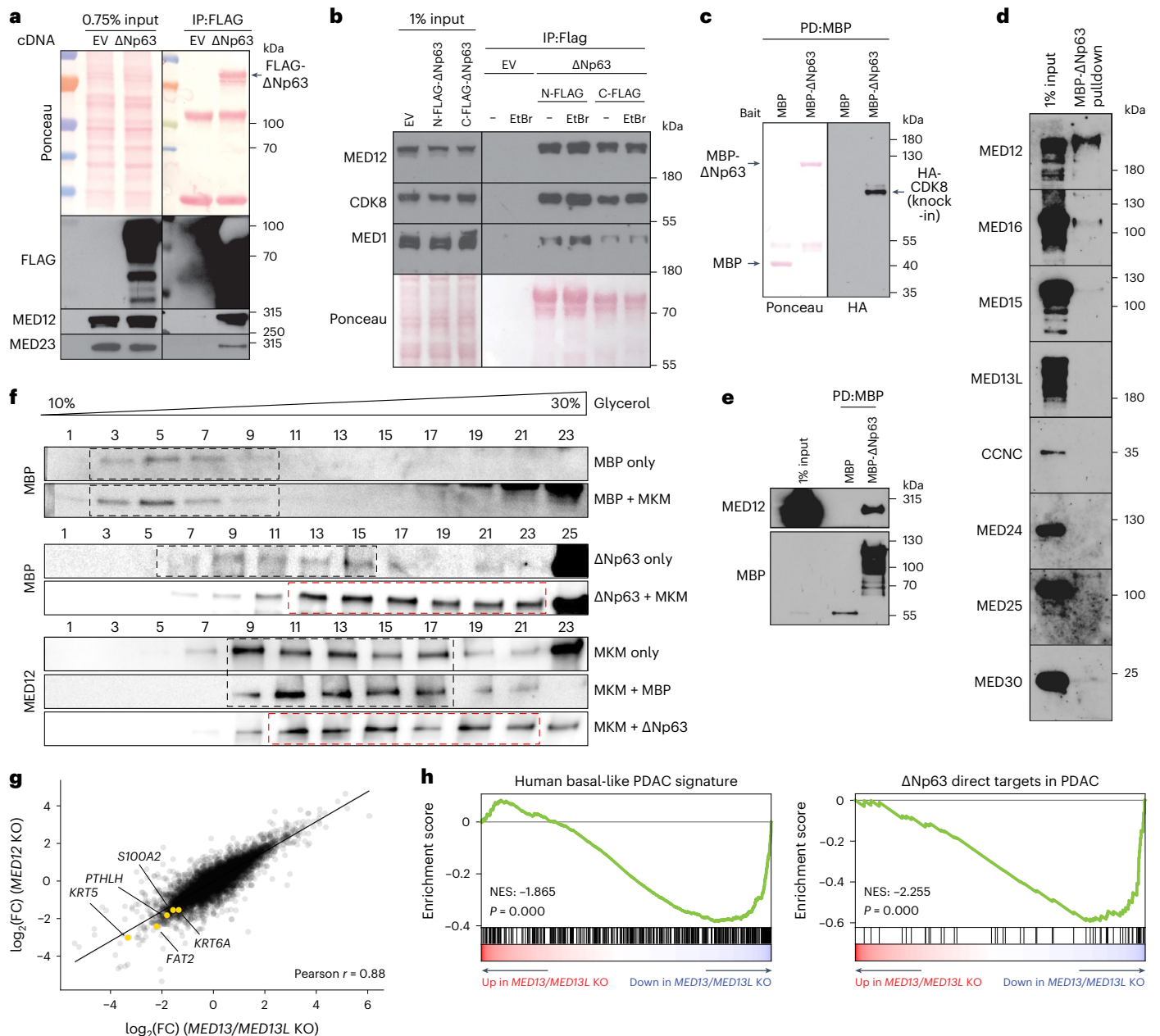
Fig. 3 | ΔNp63 directly binds to MED12 and the MKM to activate the basal lineage program. a, Representative FLAG immunoprecipitation of transiently transfected ΔNp63-C-3xFLAG in HEK293T nuclear lysates. Ponceau staining and western blot of FLAG and endogenous MKM (MED12) and core Mediator (MED23) subunits are shown for input and IP samples. **b**, FLAG immunoprecipitation of transiently transfected N-3xFLAG-ΔNp63 or ΔNp63-C-3xFLAG in HEK293T nuclear lysates in the presence or absence of EtBr (final concentration of 50 μg ml^{−1}). Ponceau and western blot of endogenous MKM (MED12, CDK8) and core Mediator (MED1) subunits are shown for input and IP samples. **c**, MBP-pulldown of purified MBP or MBP-ΔNp63 incubated with nuclear lysates of endogenously tagged N-3xHA-CDK8 HeLa cells. Ponceau (left) shows the immobilized MBP fusion proteins, and HA stains the 3xHA-tagged CDK8. Only pulldown results are shown, as no signal was detected in the 1% input. **d**, Western blot of MBP-pulldown of purified MBP-ΔNp63 incubated with Sf9 cell lysates expressing different individual human Mediator subunits. One percent input is shown in the left lane. **e**, MBP pulldown of MBP or MBP-ΔNp63 incubated with human MED12-expressing Sf9 lysates. **f**, Glycerol gradient sedimentation of purified MBP or MBP-ΔNp63 incubated with human 4-subunit MKM. Glycerol percentages are indicated above the blots; larger complexes will migrate farther down the gradient. Black dashed boxes show glycerol gradient eluted fractions of individual ΔNp63, MBP or MKM, as well as MBP-MKM incubation samples which did not display shifted migration pattern. Red dashed boxes highlight ΔNp63–MKM glycerol gradients that eluted in size-shifted fractions. **g**, Scatterplot depicting gene expression changes upon *MED12* or *MED13/MED13L* knockout. DESeq2-derived log$_2$(FC) of all substantially expressed genes in three biological replicates per sgRNA are plotted. Representative plot of two different sgRNAs per gene. Select basal genes are highlighted in yellow. **h**, GSEA plots of *MED13/MED13L* double knockout (three biological replicates per sgRNA) using gene signatures derived from human basal PDAC tumors[10] (left) and direct ΔNp63 gene targets in PDAC[18] (right). Complete GSEA for all the MKM double knockout sgRNA tested can be found in Supplementary Table 6.

Fig. 3c,d and Supplementary Table 5). Taken together, these findings suggest that MED12 occupies basal lineage enhancer elements in a p63-dependent manner.

The findings above raised the possibility that ΔNp63 binds to the MED12-containing MKM to activate transcription of basal lineage genes. When transfected into human cells, we found that
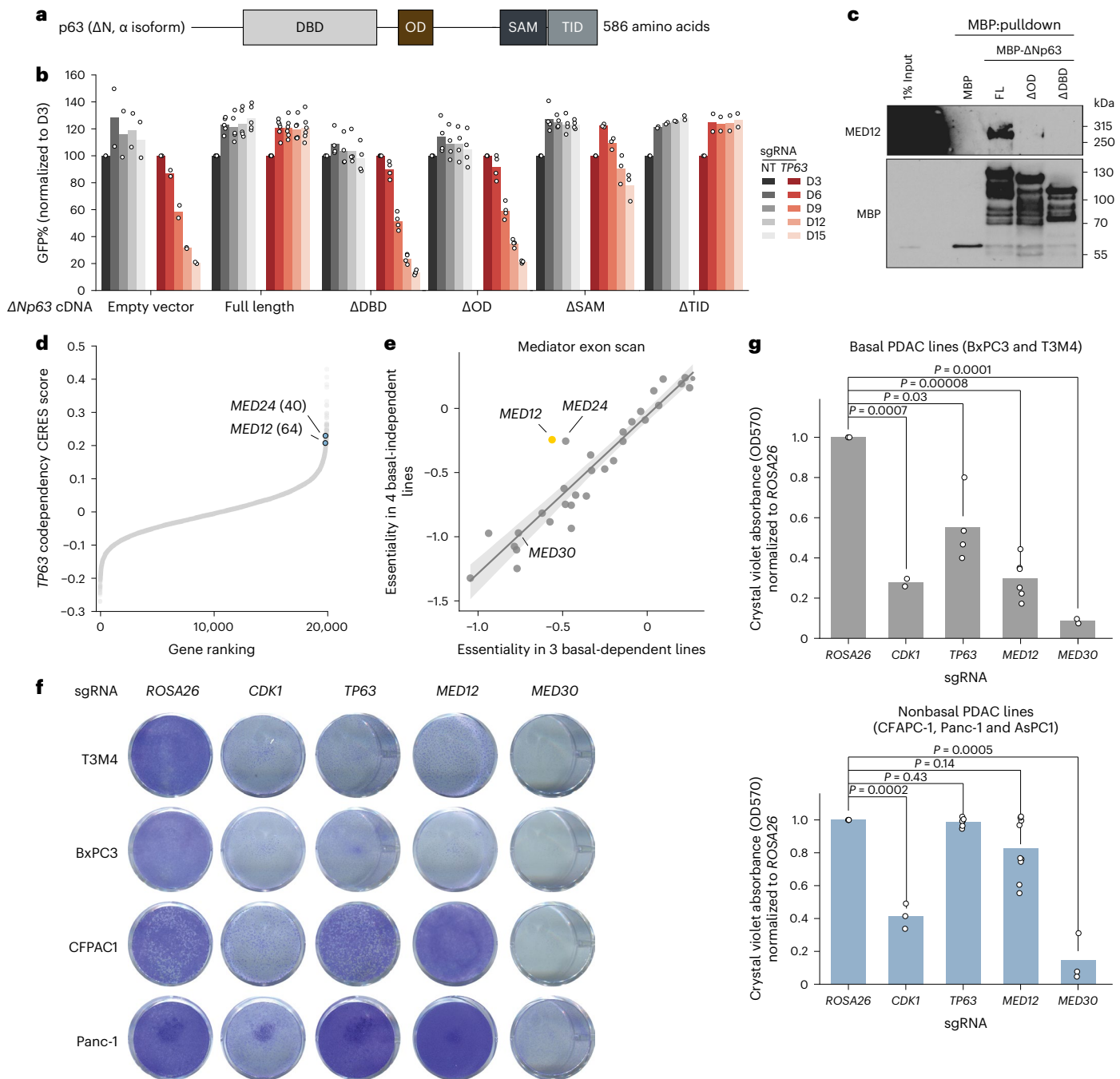
Fig. 4 | *MED12* is a lineage-biased genetic vulnerability of basal-like PDAC.
a, Diagram of ΔNp63 (N-terminus ΔN, C-terminus α isoform of p63) domain architecture. **b**, Gene complementation competition-based proliferation assay of different overexpressed ΔNp63 truncation mutants upon endogenous *TP63* CRISPRi-induced knockdown. Dots represent the average GFP% difference to day 3 GFP measurements of *n* = 2–4 biologically independent samples, and bars represent their mean. **c**, MBP pulldown assay using purified MBP, full-length MBP-ΔNp63 (FL) or MBP fusion ΔNp63 mutants lacking the oligomerization domain (ΔOD) or DNA-binding domain (ΔDBD). Purified protein was incubated with MED12-expressing Sf9 lysates overnight, followed by pulldown and western blot. **d**, Pearson *r* of >17,000 DepMap CERES gene codependencies with *TP63* across ~1,000 cell lines. **e**, Scatterplot of mean essentiality scores of all sgRNAs targeting each of 33 genes in the Mediator complex in ΔNp63-dependent (T3M4, BxPC3 and PK-1) and non-ΔNp63-dependent (SUIT2, AsPC-1, KLM1 and MiaPaCa-2) cell lines. Linear regression and 95% confidence interval are drawn. **f**, Crystal violet staining of basal (T3M4, BxPC3) or nonbasal (CFPAC1, Panc-1) human PDA lines grown for 10 days after knockout of negative control (*ROSA26*), lethal control (*CDK1*), *TP63*, *MED12* or pan-essential Mediator gene *MED30*. Additional sgRNA tested are shown in Extended Data Fig. 5c. **g**, Quantification of resolubilized crystal violet stain of basal (top: T3M4 and BxPC3) or nonbasal (bottom: CFAPC-1, Panc-1 and AsPC-1) grown for 10 days, as quantified by OD570. Dots represent independent OD570 measurements of *n* = 1–3 independent measurements per gene across basal and nonbasal cell lines, and bars represent their mean. Two-sided *t* test *P* values are shown in the figure.

FLAG-tagged ΔNp63 immunoprecipitated endogenous MED12, as well as subunits of the core Mediator and the MKM (Fig. 3a,b). This association was not affected by the presence of ethidium bromide (EtBr), suggesting it occurs in a DNA-independent manner (Fig. 3b). To evaluate this interaction in an alternative system, we expressed and purified recombinant MBP-tagged ΔNp63 from bacteria, which was

competent for oligomerization and sequence-specific DNA binding (Extended Data Fig. 4a–c). Pulldown experiments revealed that the MBP-ΔNp63 protein is efficiently associated with endogenous MKM in nuclear lysates (Fig. 3c).

To evaluate potential direct interactions between ΔNp63 and Mediator proteins, we expressed eight different human MED subunits individually in Sf9 insect cells (which lack endogenous human Mediator) and screened for an interaction with recombinant MBP-ΔNp63. Among the eight subunits tested, only MED12 bound efficiently to ΔNp63 (Fig. 3d,e). While this result suggests a direct ΔNp63–MED12 interaction, it is important to recognize that native MED12 exists as a stable subunit of the MKM. This prompted us to evaluate whether a ΔNp63–MKM complex can be reconstituted in vitro. We co-expressed human MED12, MED13, cyclin C and CDK8 in Sf9 cells and used size exclusion chromatography to isolate a stoichiometric MKM. This complex was incubated with MBP-ΔNp63 and evaluated using a glycerol gradient for a stable interaction. Notably, purified MBP-ΔNp63, but not MBP alone, was displaced toward heavier fractions of the glycerol gradient upon incubation with recombinant MKM (Fig. 3f). Together, these biochemical results suggested a direct interaction between ΔNp63 and the MED12-containing MKM.

Unexpectedly, we found that double CDK8/CDK19 knockout or treatment with CDK8/CDK19 inhibitors failed to suppress ΔNp63 target gene expression in basal-like PDAC models, despite leading to marked growth arrest (Extended Data Fig. 4d and Supplementary Tables 6 and 7). This led us to hypothesize that the critical role of MED12 as an MKM subunit might be to bridge ΔNp63 with the core Mediator, a function that is known to occur via its binding to MED13/MED13L[37]. While both MED13 and MED13L are expressed (Extended Data Fig. 4e) and were each dispensable individually for basal lineage identity (Fig. 1d), the double knockout of these two paralogs led to highly similar transcriptional changes as the loss of MED12, including effects at basal lineage genes (Fig. 3g,h, Extended Data Fig. 4f and Supplementary Table 6). While the other MKM paralog pairs display redundancy, MED12L is lowly expressed, and MED12/MED12L double knockout phenocopies the knockout of MED12 alone (Extended Data Fig. 4e–g). Of note, several core Mediator subunits also scored in our marker-based screen (Fig. 1c) and were found to be associated with ΔNp63 in nuclear lysates, which occurred independently of CDK8/CDK19 and cyclin C (Fig. 3a,b and Extended Data Fig. 4h). Collectively, our genetic, epigenomic and biochemical results support a mechanistic model in which MED12 and MED13/13L function as adaptors within the MKM that bridge ΔNp63 with the core of Mediator.

We next evaluated whether the growth of basal-like PDAC requires the interaction between MED12 and ΔNp63. To this end, we established a gene complementation assay evaluating whether different ΔNp63 cDNA constructs could rescue the growth-arrest caused by the inactivation of endogenous TP63 (Fig. 4a). Using competition-based cell fitness assays, we found that wild-type ΔNp63 and deletions of its sterile alpha motif (SAM) domain and transcription inhibition domain (TID) were still capable of supporting PDAC cell proliferation (Fig. 4b). In contrast, deletions of the DNA-binding domain (DBD) and the oligomerization domain (OD) of ΔNp63 behaved as null alleles, despite being expressed (Fig. 4b and Extended Data Fig. 5a). Guided by these results, we generated recombinant MBP-ΔNp63 ΔDBD and ΔOD proteins (Extended Data Fig. 5b). When compared to MBP-ΔNp63, both deletions abolished the interaction with MED12 in cell lysates (Fig. 4c). Taken together, these structure-function experiments suggest that the interaction between MED12 and ΔNp63 is required for the growth of basal-like PDAC cells.

To extend the findings above, we evaluated whether the growth of basal-like PDAC might be hypersensitive to the genetic knockout of MED12. Remarkably, our analysis of the cancer dependency map CRISPR screening data from >1,000 cancer cell lines[38] revealed that MED12 was in the top 1% of genetic codependencies of TP63 among

~18,600 genes that were evaluated (Fig. 4d). While the correlation between TP63 and MED12 dependencies was not linear within these data, such a correlation did not exist for most other core Mediator subunits (Supplementary Table 1). Because genome-wide CRISPR screening results can exhibit false-negative and false-positive results, we sought to perform a more rigorous validation of a potential correlation between ΔNp63 and MED12 dependencies in PDAC. For this purpose, we cloned a CRISPR tiling library that scanned 33 subunits of Mediator with all possible sgRNAs (~10,000 sgRNAs in total), which we used to perform negative-selection CRISPR screens in three ΔNp63-dependent PDAC and four ΔNp63-independent PDAC lines (Supplementary Table 8). While targeting of core Mediator subunits led to a similar pattern of growth arrest in both groups of PDAC lines, our screens revealed that MED12 was the Mediator subunit that had the strongest dependency bias toward basal-like PDAC (Fig. 4e and Supplementary Table 8). We validated this hypersensitivity using both crystal violet staining (Fig. 4f,g and Extended Data Fig. 5c), CellTiter-Glo proliferation assays (Extended Data Fig. 5d) and orthotopic transplantation experiments (Extended Data Fig. 5e–g). MED12 is required to support cell cycle progression in basal-like PDAC models (Extended Data Fig. 6a,b) and is a dependency in other non-PDAC basal/squamous carcinoma models (Extended Data Fig. 6c). Of note, these same CRISPR screening datasets identify that basal-like PDAC is hypersensitive to loss of MED24 (Fig. 4d,e and Supplementary Table 1). However, we found that this subunit does not interact with ΔNp63 in biochemical assays (Fig. 3d). This suggests that the function of MED24 is coupled to that of the MKM within the Mediator complex, a finding made independently by others[39]. While our experiments are limited by the availability of basal-like PDAC cell line models, our findings suggest that ΔNp63-dependent PDAC lines require MED12 more than ΔNp63-independent PDAC, despite sharing a similar dependency on core Mediator subunits.

Lineage plasticity is widely recognized as a phenotypic hallmark of human cancer that allows tumor cells to gain metastatic potential and evade therapy[1]. Recent advances in single-cell transcriptomics and lineage tracing have provided unparalleled insights into this process[40,41]. However, a major challenge exists in discovering perturbations that restrain cellular plasticity in human tumors. Building upon prior work evaluating smaller gene sets[18,20,23,42–44], our study describes a genome-wide screening strategy that allows for the comprehensive mapping of genetic requirements to sustain an aberrant lineage state in PDAC. We anticipate that the methodology described here can be readily adapted to other clinically relevant tumor plasticity phenomena, such as adenocarcinomas that transition into neuroendocrine or mesenchymal cell states[2]. As many actionable targets for cancer therapeutics are ubiquitously expressed proteins across cell types, their involvement in lineage plasticity might only be revealed through high-throughput genetic perturbations. Our study also demonstrates how marker-based genetic screens can be leveraged to reveal a highly specific protein–protein interaction that functions as a lineage-biased cancer dependency. In this regard, the reconstituted interaction between ΔNp63 and MKM could be readily adapted into a biochemical assay for high-throughput chemical screening. Thus, our integrated experimental approach combining genetics and biochemistry may have biomedical utility to advance pharmacology that rewires cancer cell plasticity for therapeutic gain.

Online content

Any methods, additional references, Nature Portfolio reporting summaries, source data, extended data, supplementary information, acknowledgements, peer review information; details of author contributions and competing interests; and statements of data and code availability are available at https://doi.org/10.1038/s41588-024-01790-y.

References

1. Hanahan, D. Hallmarks of cancer: new dimensions. *Cancer Discov.* **12**, 31–46 (2022).
2. Quintanal-Villalonga, Á. et al. Lineage plasticity in cancer: a shared pathway of therapeutic resistance. *Nat. Rev. Clin. Oncol.* **17**, 360–371 (2020).
3. Badve, S. et al. Basal-like and triple-negative breast cancers: a critical review with an emphasis on the implications for pathologists and oncologists. *Mod. Pathol.* **24**, 157–167 (2011).
4. Risom, T. et al. Differentiation-state plasticity is a targetable resistance mechanism in basal-like breast cancer. *Nat. Commun.* **9**, 3815 (2018).
5. Choi, W. et al. Identification of distinct basal and luminal subtypes of muscle-invasive bladder cancer with different sensitivities to frontline chemotherapy. *Cancer Cell.* **25**, 152–165 (2014).
6. Choi, W. et al. p63 expression defines a lethal subset of muscle-invasive bladder cancers. *PLoS ONE* **7**, e30206 (2012).
7. Collisson, E. A. et al. Subtypes of pancreatic ductal adenocarcinoma and their differing responses to therapy. *Nat. Med.* **17**, 500–503 (2011).
8. Moffitt, R. A. et al. Virtual microdissection identifies distinct tumor- and stroma-specific subtypes of pancreatic ductal adenocarcinoma. *Nat. Genet.* **47**, 1168–1178 (2015).
9. Bailey, P. et al. Genomic analyses identify molecular subtypes of pancreatic cancer. *Nature* **531**, 47–52 (2016).
10. Chan-Seng-Yue, M. et al. Transcription phenotypes of pancreatic cancer are driven by genomic events during tumor evolution. *Nat. Genet.* **52**, 231–240 (2020).
11. Hsieh, M.-S., Jhuang, J.-Y., Hua, S.-F. & Chou, Y.-H. Histologic evolution from adenocarcinoma to squamous cell carcinoma after gefitinib treatment. *Ann. Thorac. Surg.* **99**, 316–319 (2015).
12. Awad, M. M. et al. Acquired resistance to KRASG12C inhibition in cancer. *N. Engl. J. Med.* **384**, 2382–2393 (2021).
13. Senoo, M., Pinto, F., Crum, C. P. & McKeon, F. p63 is essential for the proliferative potential of stem cells in stratified epithelia. *Cell* **129**, 523–536 (2007).
14. Ramsey, M. R. et al. FGFR2 signaling underlies p63 oncogenic function in squamous cell carcinoma. *J. Clin. Invest.* **123**, 3525–3538 (2013).
15. Como, C. J. D. et al. p63 expression profiles in human normal and tumor tissues. *Clin. Cancer Res.* **8**, 494–501 (2002).
16. Martens, S. et al. Discovery and 3D imaging of a novel ΔNp63-expressing basal cell type in human pancreatic ducts with implications in disease. *Gut* **71**, 2030–2042 (2022).
17. Hayashi, A. et al. A unifying paradigm for transcriptional heterogeneity and squamous features in pancreatic ductal adenocarcinoma. *Nat. Cancer* **1**, 59–74 (2020).
18. Somerville, T. D. D. et al. TP63-mediated enhancer reprogramming drives the squamous subtype of pancreatic ductal adenocarcinoma. *Cell Rep.* **25**, 1741–1755 (2018).
19. Collisson, E. A., Bailey, P., Chang, D. K. & Biankin, A. V. Molecular subtypes of pancreatic cancer. *Nat. Rev. Gastroenterol. Hepatol.* **16**, 207–220 (2019).
20. Hamdan, F. H. & Johnsen, S. A. DeltaNp63-dependent super enhancers define molecular identity in pancreatic cancer by an interconnected transcription factor network. *Proc. Natl Acad. Sci. USA* **115**, 201812915 (2018).
21. Somerville, T. D. et al. Squamous *trans*-differentiation of pancreatic cancer cells promotes stromal inflammation. *eLife* **9**, e53381 (2020).
22. Danilov, A. V. et al. DeltaNp63alpha-mediated induction of epidermal growth factor receptor promotes pancreatic cancer cell growth and chemoresistance. *PLoS ONE* **6**, e26815 (2011).
23. Andricovich, J. et al. Loss of KDM6A activates super-enhancers to induce gender-specific squamous-like pancreatic cancer and confers sensitivity to BET inhibitors. *Cancer Cell* **33**, 512–526 (2018).
24. Brody, J. R. et al. Adenosquamous carcinoma of the pancreas harbors KRAS2, DPC4 and TP53 molecular alterations similar to pancreatic ductal adenocarcinoma. *Mod. Pathol.* **22**, 651–659 (2009).
25. Luyties, O. & Taatjes, D. J. The Mediator kinase module: an interface between cell signaling and transcription. *Trends Biochem. Sci.* **47**, 314–327 (2022).
26. Pelish, H. E. et al. Mediator kinase inhibition further activates super-enhancer-associated genes in AML. *Nature* **526**, 273–276 (2015).
27. Freitas, K. A. et al. Enhanced T cell effector activity by targeting the Mediator kinase module. *Science* **378**, eabn5647 (2022).
28. Chu, P. G. & Weiss, L. M. Expression of cytokeratin 5/6 in epithelial neoplasms: an immunohistochemical study of 509 cases. *Mod. Pathol.* **15**, 6–10 (2002).
29. Kokumai, T. et al. GATA6 and CK5 stratify the survival of patients with pancreatic cancer undergoing neoadjuvant chemotherapy. *Mod. Pathol.* **36**, 100102 (2023).
30. Basturk, O. et al. DeltaNp63 expression in pancreas and pancreatic neoplasia. *Mod. Pathol.* **18**, 1193–1198 (2005).
31. Horlbeck, M. A. et al. Compact and highly active next-generation libraries for CRISPR-mediated gene repression and activation. *eLife* **5**, e19760 (2016).
32. Raghavan, S. et al. Microenvironment drives cell state, plasticity, and drug response in pancreatic cancer. *Cell* **184**, 6119–6137 (2021).
33. Antonini, D. et al. An autoregulatory loop directs the tissue-specific expression of p63 through a long-range evolutionarily conserved enhancer. *Mol. Cell. Biol.* **26**, 3308–3318 (2006).
34. Antonini, D. et al. A composite enhancer regulates p63 gene expression in epidermal morphogenesis and in keratinocyte differentiation by multiple mechanisms. *Nucleic Acids Res.* **43**, 862–874 (2015).
35. Doench, J. G. et al. Optimized sgRNA design to maximize activity and minimize off-target effects of CRISPR–Cas9. *Nat. Biotechnol.* **34**, 184–191 (2016).
36. Tiriac, H. et al. Organoid profiling identifies common responders to chemotherapy in pancreatic cancer. *Cancer Discov.* **8**, 1112–1129 (2018).
37. Tsai, K.-L. et al. A conserved Mediator–CDK8 kinase module association regulates Mediator–RNA polymerase II interaction. *Nat. Struct. Mol. Biol.* **20**, 611–619 (2013).
38. Behan, F. M. et al. Prioritization of cancer therapeutic targets using CRISPR–Cas9 screens. *Nature* **568**, 511–516 (2019).
39. Bell, C. C. et al. Transcription factors use a unique combination of cofactors to potentiate different promoter-dependent steps in transcription. Preprint at *bioRxiv* https://doi.org/10.1101/2022.10.25.513774 (2022).
40. Yang, D. et al. Lineage tracing reveals the phylodynamics, plasticity, and paths of tumor evolution. *Cell.* **185**, 1905–1923 (2022).
41. Chan, J. M. et al. Lineage plasticity in prostate cancer depends on JAK/STAT inflammatory signaling. *Science* **377**, 1180–1191 (2022).
42. Miyabayashi, K. et al. Intraductal transplantation models of human pancreatic ductal adenocarcinoma reveal progressive transition of molecular subtypes. *Cancer Discov.* **10**, 1566–1589 (2020).
43. Brunton, H. et al. HNF4A and GATA6 loss reveals therapeutically actionable subtypes in pancreatic cancer. *Cell Rep.* **31**, 107625 (2020).

44. Kloesch, B. et al. A GATA6-centred gene regulatory network involving HNFs and ΔNp63 controls plasticity and immune escape in pancreatic cancer. *Gut* **71**, 766–777 (2021).

Publisher's note Springer Nature remains neutral with regard to jurisdictional claims in published maps and institutional affiliations.

Methods

Institutional approval
This study complies with all relevant ethical regulations. Experimental protocols involving mice were approved by the Institutional Animal Care and Use Committee at Cold Spring Harbor Laboratory.

Human 2D cancer cell lines and tissue culture
T3M4 (RCB1021), KLM1 (RCB2138), AsPC-1 (ATCC, CRL-1682), PK-1 (RCB1972), BxPC3 (ATCC, CRL-1687), HCC1806 (ATCC, CRL-2335), Hsc5 (ATCC, CRL-3611), Cal33 (DSMZ, ACC 447), KYSE70 (DSMZ, ACC 363) and KYSE410 cells (DSMZ, ACC 381) were cultured in Roswell Park Memorial Institute Medium supplemented with 10% FBS and penicillin/streptomycin (R10). SUIT2 (JCRB1094), CFPAC1 (ATCC, CRL-1918), PANC1 (ATCC, CRL-1469), MIAPaCa-2 (ATCC, CRL-1420) and HeLa cells were cultured in DMEM supplemented with 10% FBS and penicillin/streptomycin (D10). Cell lines were purchased from commercial vendors, and their identities were validated by short tandem repeat analysis. Cell lines were regularly tested for *Mycoplasma* contamination. All antibiotic concentrations used to select gene cassettes were empirically titrated in each cell line to achieve maximum selection with minimum toxicity.

Human organoid tissue culture
hF3 PDAC[36] and NH93T triple-negative breast cancer[45] patient-derived organoids were grown in 3D Matrigel domes in hCPLT or complete breast cancer organoid media and cultured as described previously[36,45]. Briefly, organoids were first collected in cold Advanced DMEM/F-12. They were subsequently pelleted by centrifugation at 300g for 5 min, dissociated to single cells by incubation in 1× TrypLE for 15 min at 37 °C, washed once with Advanced DMEM/F-12 and resuspended in 100% Matrigel (Corning, 356255) for plating.

Intracellular FACS-based CRISPR screens
CRISPR screens were conducted as described previously. Briefly, after determining the suitable lentiviral titer, ~1 to 2×10^9 Cas9-expressing cells were seed-infected at D0 with genome-wide CRISPRi[31] or knock-out[35] sgRNA library-encoding lentiviral suspension for a final 20–30% GFP+ percentage of infected cells. Media was changed at 48 h, and puromycin was added for 72 h for sgRNA cassette integration selection. After 6 days of infection, cells were resuspended in trypsin, counted, washed in cold PBS and fixed in −20 °C methanol at 10×10^6 cells per ml under gentle vortexing. Cells were stored in methanol at −20 °C for a period of up to 4 months. The day before sorting, cells were pelleted, washed once in FACS buffer (1% (wt/vol) ultrapure BSA, 0.5% (wt/vol) sodium azide and 1 mM EDTA in magnesium and calcium-free PBS) and incubated overnight in 1:400 primary antibody (KRT5 or p63) in FACS buffer at 10×10^6 cells per ml rotating at 4 °C. The next day, cells were pelleted, washed twice with FACS buffer and incubated for 1–2 h in 1:500 secondary antibody (AF647-conjugated goat anti-rabbit) in FACS buffer at 10×10^6 cells per ml rotating at 4 °C protected from light. After washing twice in FACS buffer, cells were resuspended in FACS buffer to ~10×10^6 cells per ml and sorted. Stained cells were sorted using a BD FACSAria II cell sorter. The total number of cells sorted per screen was a minimum of 1,500× the size of the sgRNA library. Cells were sorted into three different pools, with approximately 30% of cells sorted into the marker[low] bin and 15% sorted into the marker[high] bin. Cell pellets were then processed for DNA extraction and library preparation. A custom sequencing primer was added for next-generation sequencing of all CRISPRi screens, as described previously[31]. All sequencing data from FACS-based genome-wide screens analyzed using MAGeCK v0.5.9.3 (ref. 46) with the maximum likelihood estimation option.

Mediator exon scan library construction and cloning
sgRNA sequences targeting all 33 possible human Mediator subunits were retrieved from the CSHL in-house CRISPR sgRNA design tool, the VBC score sgRNA database and the Broad Institute CRISPick tool. Duplicate sgRNAs were removed, and all other remaining guides plus 391 nontargeting sgRNAs were incorporated into the final library pool (10,000 sgRNA). All sgRNA sequences are available in Supplementary Table 8.

Pooled amplicons with overhangs were ordered from Twist Bioscience, and cloned into the LRG-Puromycin (Addgene, 125594) backbone using the NEBuilder HiFi DNA assembly master mix. The purified product was electroporated into MegaX DH10B (Invitrogen) and plated into LB-carbenicillin plates with a minimum representation of 100 colonies per sgRNA. The colonies were scraped from the plates, and their DNA was extracted using Invitrogen MaxiPrep kit. Libraries were amplified for ten cycles and sequenced to confirm successful cloning.

Negative selection Mediator exon scanning CRISPR screens
A total of ~1×10^8 Cas9-expressing cells were seed-infected with the Mediator exon scanning lentiviral sgRNA library to ~20 to 30% by GFP+ population at day 3. At day 2 post-infection, ~5×10^7 cells were collected and flash frozen for early timepoint, and the remaining cells were puromycin-selected for 72 h. Cells were subsequently passaged every 3 days for a period of 15 days, maintaining a minimum of ~5×10^7 infected cells in culture at any given time. After 15 days (late timepoint), ~5×10^7 cells were collected. Early and late timepoint cell pellets were subjected to DNA extraction as detailed below, and their sgRNA cassettes were sequenced. sgRNA depletion scores were calculated from raw sequencing files using MAGeCK v0.5.9.3 (ref. 46) with the option RRA. Downstream analysis was done in Python 3.6.

DNA extraction and sgRNA-seq for CRISPR screens
After sorting, cells from each sorting bin were pelleted and pooled, and their DNA was extracted as follows. Cells were resuspended in DNA extraction buffer (10 mM Tris–HCl pH 8, 150 mM NaCl and 10 mM EDTA) at a density of 12.5 M cells per ml. SDS and proteinase K were added to final concentrations of 0.1% and 0.2 mg ml^{-1}, respectively. The mixture was incubated for 48 h at 56 °C, after which DNA was purified by phenol extraction. Equilibrated phenol was added 1:1 to the lysis mixture, mixed well and centrifuged for 10 min at 20,000 RCF. The supernatant was carefully removed, and another round of phenol purification was performed. DNA was then precipitated by adding three volumes of isopropanol and NaOAc pH 5.2 to a final concentration of 75 mM and incubating overnight at −20 °C. DNA was then pelleted at maximum speed for 1 h, washed in 70% ethanol and air-dried until translucent. After resuspension in water, DNA was assessed for quality by Nanodrop before proceeding to library prep.

sgRNA was directly amplified from genomic DNA in one-step PCR using NEBNext Ultra II Q5 Master Mix (NEB). Each PCR reaction was done with 10 μg of genomic DNA in a 100-μl final volume. Titrations of amplification cycles were performed for Lenti_sgRNA_EFS_GFP (95 °C, 1 min; n cycles (95 °C, 30 s; 53 °C, 30 s; 72 °C, 30 s); 72 °C, 10 min) and CRISPRi (98 °C, 30 s; n cycles (98 °C, 10 s; 65 °C, 75 s); 65 °C, 5 min) sgRNA backbone vectors, which showed they could both be efficiently amplified using 22 cycles. All PCR reactions for each sample were pooled, and 400 μl of the amplified mix was taken for double-sided Ampure bead cleanup (0.65× + 1× bead volume) to preserve sgRNA PCR amplicons (~354 bp and ~274 bp, respectively). Amplicons were sequenced using Illumina NextSeq with 50% spike-in or pooled with unrelated high-diversity libraries (Cold Spring Harbor Genome Center).

General computational and statistical analysis
All sequencing data were analyzed using CSHL high-performance computing system. Packages used to analyze next-generation sequencing data were installed in independent Anaconda environments to minimize conflicts of dependencies. Downstream analysis was performed using Python 3.6 in JupyterLab notebooks. Statistical tests and regressions were done using Scipy and Seaborn, respectively.

RNA-seq data analysis

Single-end 76-bp raw sequencing reads were mapped to the hg38 genome using STAR v2.7.9a[47], followed by HTSeq v2.21 (ref. [48]) to generate raw gene counts. Low abundance transcripts were filtered out (<2 average raw counts), and normalized expression values (variant stabilized transcripts) and differential expression values were calculated using DESeq2 (ref. [49]). Two to three biological replicates per sgRNA per cell line were tested.

Gene set enrichment analysis (GSEA) and plotting were conducted using GSEApy v1.0.0 (ref. [50]). GSEA was performed using DESeq2-generated variant stabilized transformed counts of each tested sample in duplicates or triplicates and the permutation 'gene set' option. Gene signatures for human basal PDAC were retrieved from signature 10 (basal A) of ref. [10], and for direct ΔNp63 target genes in PDAC from ref. [21]. GSEA normalized enrichment scores and *P* values calculated for all RNA-seq samples of this study, as well as the list of genes in each signature used, are displayed in Supplementary Tables 3, 4, 6 and 7.

ChIP–seq analysis

Single-end 76-bp sequencing reads were mapped to the hg38 genome using Bowtie2 (ref. [51]) with default settings. MACS v2.2.6 (ref. [52]) was used to call peaks using input genomic DNA as control. Annotation of ChIP–seq peaks was performed using HOMER v4.11 with default settings[53]. To visualize genomic tracks, bigWig files were generated from BAM files using deepTools v3.5.0 (ref. [54]) bamCoverage-RPCG function normalizing with reads per genome coverage. To define BED files of peaks and peak overlaps, MACS2 output narrowPeak or broadPeak files were merged using bedtools v2.30.0 (ref. [55]) merge and intersect tools. Heatmaps and average chromatin occupancy metaplots were generated using computeMatrix and plotHeatmap functions of deepTools, taking bigWig files and BED files as input.

For ChIP–seq analysis of KLM1 *TP63* KO, MED12 peaks were merged between all KLM1 samples and intersected with a list of basal lineage enhancers retrieved from ref. [18] using bedtools. The resulting 453 loci were evaluated for MED12 and ΔNp63 abundance upon *ROSA26* or *TP63* KO using deepTools. For SUIT2 CRISPRa *TP63*, MED12 peaks were merged between all SUIT2 samples and annotated using HOMER. A total of 80 MED12 peaks whose nearest genes intersect with ΔNp63 direct target genes from ref. [18] were used to generate metaplots of all SUIT2 CRISPRa conditions centered around these loci. All custom *cis*-regulatory elements defined in this study are shown in Supplementary Table 5.

Orthotopic injection and luciferase imaging of basal and nonbasal PDAC

NOD.Cg-Prkdc scid Il2rg tm1Wjl /SzJ (NSG; The Jackson Laboratory, 005557) 8–10-week-old female mice (*Mus musculus*) were used for orthotopic injections (four mice per group). Gene knockout T3M4 or Panc-1 cells were generated as described in the Supplementary Note. Just before injection, cells were resuspended in a 50/50 mixture of PBS and Matrigel at a concentration of 3,750,000 cells per ml. Under a sterile environment, the left lateral side of NSG mice was shaved, and residual fur was removed with Nair. Mice were anesthetized with isoflurane and given a subcutaneous injection of buprenorphine according to CSHL animal handling guidelines. Next, a vertical incision was made inferior to the rib cage on the left side, exposing the tissue overlying the spleen. The tissue overlaying the spleen was incised, and the spleen was gently retracting, exposing the body of the pancreas. Using a 31G insulin syringe (BD Biosciences, 324903), 20 µl of the cell mixture (75,000 cells) was injected into the body of the pancreas. A bubble in the pancreas was noted, indicating an injection that did not leak. The peritoneal cavity was then closed with dissolving sutures (Thermo Fisher Scientific, 50-209-2818), and the skin was closed with wound clips (VWR, 203-1000). Topical lidocaine was applied to the skin, and the mice were then incubated in a heated recovery chamber before returning them to their cage. Mice were monitored for 2 days post-surgery and treated with additional analgesics as needed, according to the CSHL animal surgical guidelines. Wound clips were removed before 2 weeks post-surgery.

For luciferase imaging, mice were first anesthetized with isoflurane and then intraperitoneally injected with 200 µl of luciferin (50 mg kg^{-1}) into the lower right quadrant with a 27G needle (BD Biosciences, 30519). Fifteen minutes were allowed to pass, and bioluminescence was imaged with an IVIS Spectrum (Xenogen). Experimental protocols involving mice were approved by the Institutional Animal Care and Use Committee at Cold Spring Harbor Laboratory.

Bacterial expression and purification of recombinant MBP-p63

MBP-6xHis-TEV-p63 expression was induced in BL21 cells grown in Luria broth supplemented with antibiotics and 0.5 mM IPTG for 18 h at 16 C. Cells were collected by centrifugation at 4,000 RCF for 10 min at 4 °C, resuspended in 30 ml of lysis buffer (50 mM Tris pH 7.5, 150 mM KCl, 5 mM MgCl$_2$, 0.05% NP-40, 10% glycerol, 0.2 mM EDTA, 1 mM DTT (fresh)) and supplemented with protease inhibitors and 100 µg ml^{-1} lysozyme. After 45 min of incubation on ice, cells were sonicated for 2 min and 30 s (3 s on, 5 s off) with a probe sonicator. Lysates were clarified by ultracentrifugation at 100,000 RCF for 1 h at 4 °C. Cleared bacterial lysate from 1 l of culture was incubated with 2 ml of equilibrated amylose resin (NEB, E8021L) in a rotator overnight at 4 °C. The next day, the resin was pelleted, washed once in 50 ml of wash buffer (50 mM Tris pH 7.5, 500 mM KCl, 5 mM MgCl$_2$, 0.05% NP-40, 10% glycerol, 1 mM DTT (fresh)) and resuspended in 15 ml of lysis buffer. After passing the lysate and resin mix through a chromatography column, the protein was eluted in five fractions of 1 ml of elution buffer (20 mM maltose in lysis buffer). A size exclusion purification step was followed using an AKTA Pure 25 M (Cytiva 29018226) using a Superdex 200 Increase 10/300 GL. Purity was evaluated by SDS-PAGE and Coomassie staining, and protein was flash frozen in liquid nitrogen and kept at −80 °C. All purified proteins were validated by mass spectrometry peptide identification and western blot.

Sf9 expression and purification of recombinant human MKM and other Mediator genes

Each individual Mediator subunit was cloned and expressed in a pLIB plasmid (Addgene, 80610). *MED12*, *MED13L*, Twin-Strep-*CDK8* and *CCNC* were cloned into a multiBac vector and subsequently used to generate bacmid with the EmBacY vector (Geneva Biotech). To generate baculovirus, Sf9 cells were transfected with TransIT-insect transfection reagent (Mirus) and 5–10 µg of plasmid following the manufacturer's instructions. A baculovirus amplification round was then performed with this supernatant using 200 ml of Sf9 in suspension culture seeded at 10^6 per ml and grown for 48–72 h. Here 20–50 ml of baculovirus was used to infect 1 l of Sf9 for protein expression. The cultures were grown for 48–72 h, at which point cells were collected by centrifugation. Pellets were kept frozen at −80 °C or proceeded immediately for protein extraction. For protein isolation, pellets were resuspended in lysis buffer (25 mM HEPES pH 7.5, 100 mM KCl, 0.05% NP-40 and 10% glycerol) and Dounce homogenized 40 times on ice using pestle A. Debris was removed by ultracentrifugation at 100,000*g* for 1 h at 4 °C, and the supernatant was either flash frozen or subjected to further purification. For MKM purification, twin-strep-tagged MKM containing lysates were incubated with Streptactin XT magnetic bead slurry (IBA Lifesciences) and purified according to the manufacturer's recommendation. Further purification using a glycerol gradient was performed before experiments where high purity was required. Protein preparations were evaluated by SDS-PAGE and Coomassie or silver staining, and protein was flash frozen in liquid nitrogen and kept at −80 °C.

Glycerol gradients

Glycerol gradients were prepared using a peristaltic pump and precooled base buffers (10–30% glycerol, 20 mM 7.6 HEPES-HCl, 150 mM

KCl, 0.02% NP-40 and 0.1 mM EDTA). Lysates and/or purified proteins in a maximum volume of 500 µl were incubated for 3 h before immunoprecipitating and carefully layering the elutions on top of a freshly poured 2.4 ml glycerol gradient. Samples were ultracentrifuged in a TLS 55 rotor at 35,000 rpm for 16 h at 4 °C, with the standard acceleration and deceleration speed settings. Here 100 µl fractions were successively taken from the top layer without disrupting the column, evaluated by Coomassie, silver stain and/or western blot, and taken to further processing and experimenting.

Immunoprecipitation
HEK293T cells were collected by trypsinization or scraping and washed once with ice-cold PBS. Cells were then incubated with 2 ml of cell lysis buffer (25 mM HEPES pH 7.5, 10 mM KCl, 1.5 mM $MgCl_2$, 0.05% NP-40, 15% glycerol, 1 mM DTT (fresh), protease inhibitors (fresh)) per 10 cm dish of cells for 10 min. Nuclei were then pelleted for 5 min at 3,000 RCF and incubated in nuclear extraction buffer (25 mM HEPES pH 7.5, 150 mM KCl, 1.5 mM $MgCl_2$, 0.05% NP-40, 2 mM HEPES pH 7.5) for 30 min. Nuclear lysates were cleared by centrifugation at 20,000 RCF for 1 h and subsequently incubated with magnetic M2 FLAG beads overnight on a rotator. After washing four times with 1 ml of nuclear extraction buffer, beads were resuspended in 50 µl of nuclear extraction buffer. After adding 50 µl of 2× Laemmli buffer, samples were boiled for 10 min at 98 °C, and run on an SDS-PAGE gel for western blotting. Except for the sample boiling, all steps were performed at 4 °C.

MBP pulldown
Magnetic amylose bead slurry (50–100 µl) was equilibrated in 20–40 volumes of lysis buffer (20 mM HEPES pH 7.5, 150 mM KCl, 0.05% NP-40%) and incubated with MBP or MBP-tagged protein for 2–3 h. After washing once with 10–20 volumes of lysis buffer, the protein–resin mix was incubated with precleared nuclear lysates or purified protein overnight. After washing four times with 10–20 volumes of lysis buffer, the resin was resuspended in 100 µl of lysis buffer supplemented with 20 mM of maltose. The mixture was incubated for 30 min on a nutator, after which the eluate was separated from the resin and boiled at 98 °C for 5 min in 1× Laemmli buffer. Except for the sample boiling, all steps were performed at 4 °C.

Antibodies and protein reagents
All antibodies and protein-binding matrices, as well as their concentrations for each application, can be found in Supplementary Table 11.

Reporting summary
Further information on research design is available in the Nature Portfolio Reporting Summary linked to this article.

Data availability
All genomic datasets are available at the Gene Expression Omnibus database under accession code GSE229062. KLM1 H3K27ac, BxPC3 *TP63* knockout and SUIT2 ΔNp63 overexpression ChIP–seq data in Extended Data Fig. 1b were obtained from previous studies[18,21]. The cancer dependency and expression datasets were obtained online at https://depmap.org/portal/download/ (DepMap Public 21Q4).

Code availability
No custom code was generated for this study. Details of all software packages used for data processing and analysis are provided in the appropriate section of Methods.

References
45. Bhatia, S. et al. Patient-derived triple-negative breast cancer organoids provide robust model systems that recapitulate tumor intrinsic characteristics. *Cancer Res.* **82**, 1174–1192 (2022).
46. Li, W. et al. MAGeCK enables robust identification of essential genes from genome-scale CRISPR/Cas9 knockout screens. *Genome Biol.* **15**, 554 (2014).
47. Dobin, A. et al. STAR: ultrafast universal RNA-seq aligner. *Bioinformatics* **29**, 15–21 (2013).
48. Putri, G. H., Anders, S., Pyl, P. T., Pimanda, J. E. & Zanini, F. Analysing high-throughput sequencing data in Python with HTSeq 2.0. *Bioinformatics* **38**, 2943–2945 (2022).
49. Love, M. I., Huber, W. & Anders, S. Moderated estimation of fold change and dispersion for RNA-seq data with DESeq2. *Genome Biol.* **15**, 550 (2014).
50. Fang, Z., Liu, X. & Peltz, G. GSEApy: a comprehensive package for performing gene set enrichment analysis in Python. *Bioinformatics* **39**, btac757 (2022).
51. Langmead, B. & Salzberg, S. L. Fast gapped-read alignment with Bowtie 2. *Nat. Methods* **9**, 357–359 (2012).
52. Zhang, Y. et al. Model-based analysis of ChIP–seq (MACS). *Genome Biol.* **9**, R137 (2008).
53. Heinz, S. et al. Simple combinations of lineage-determining transcription factors prime *cis*-regulatory elements required for macrophage and B cell identities. *Mol. Cell.* **38**, 576–589 (2010).
54. Ramírez, F. et al. deepTools2: a next generation web server for deep-sequencing data analysis. *Nucleic Acids Res.* **44**, W160–W165 (2016).
55. Quinlan, A. R. & Hall, I. M. BEDTools: a flexible suite of utilities for comparing genomic features. *Bioinformatics* **26**, 841–842 (2010).

Author contributions
D.M.-S. and C.R.V. conceived this project, designed the experiments and wrote the paper with input from all of the authors. D.M.-S. performed the experiments and analyzed the data with the following help: A.C.S. isolated MKM and performed glycerol gradients in Fig. 3f; D.S. conducted cell culture and cell sorting for basal lineage CRISPR screens; P.J.C. performed scRNA-seq and non-PDAC RNA-seq and western blot experiments; M.C.T. analyzed scRNA-seq data and C.O.d.S. provided advice; P.M. and X.Y.H. performed orthotopic transplantation experiments and D.T.F. and M.E. provided advice; Y.G. performed flow cytometry cell cycle and MKM knockout pulldown experiments; V.K. performed knockdown RNA-seq and cell proliferation competition experiments; D.L.S. provided advice on basal breast organoids; Y.S. performed culturing and experiments on breast organoids; L.W. performed non-PDAC western blot experiments and A.R.K. provided advice; A.A. and J.L. helped establish systems for Mediator complex expression in Sf9; C.R.V. and D.J.T. supervised the studies. C.R.V. acquired the funding.

Competing interests
C.R.V. has received consulting fees from Flare Therapeutics, Roivant Sciences and C4 Therapeutics; has served on the advisory boards of KSQ Therapeutics, Syros Pharmaceuticals and Treeline Biosciences;

Additional information
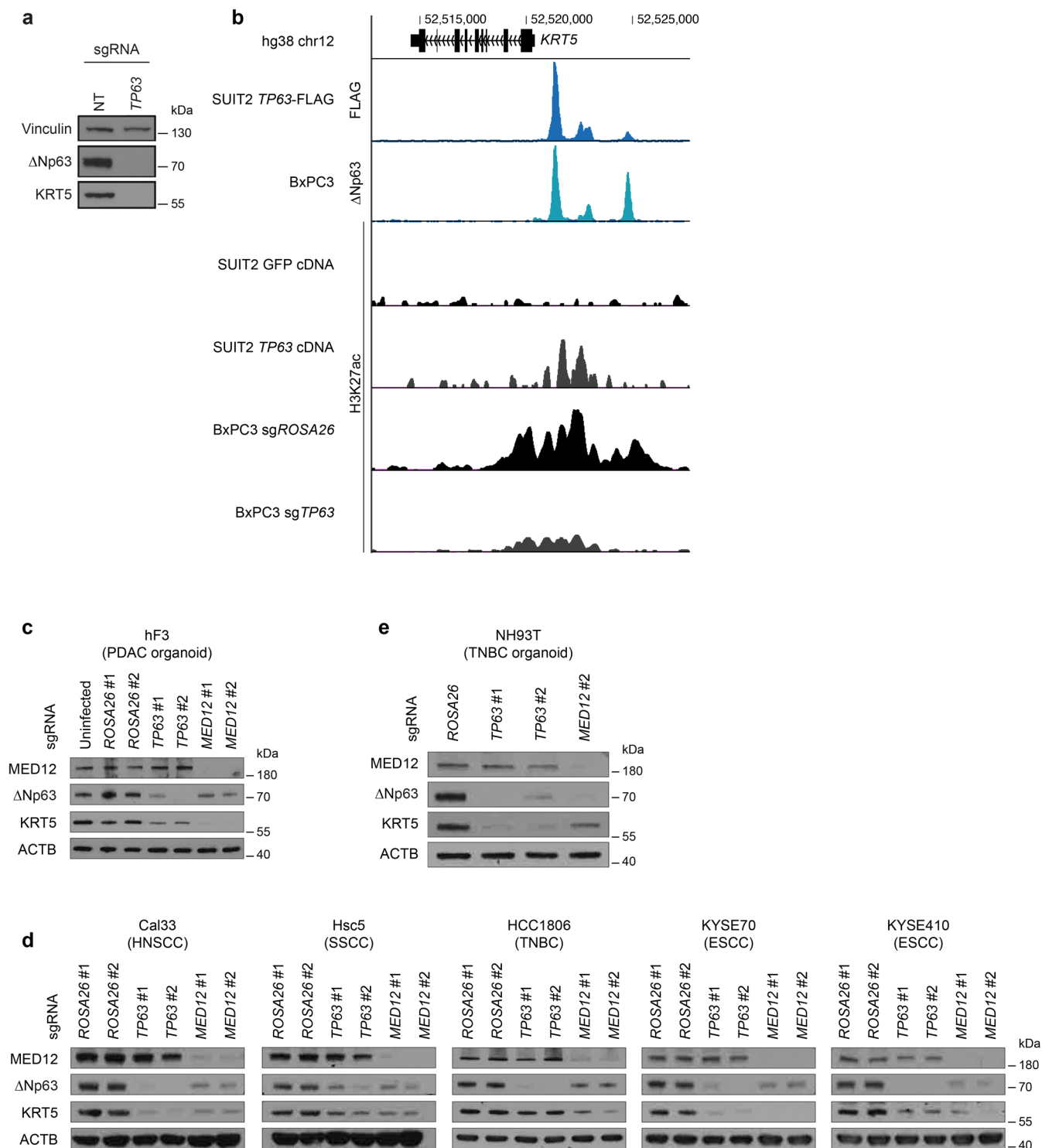
Extended Data Fig. 1 | KRT5 expression is directly regulated by ΔNp63 and MED12 controls basal marker gene expression. a, Western blot of CRISPRi-mediated *TP63* knockdown in KLM1 cells. **b**, ChIP–seq genomic occupancy tracks[18] zoomed in the *KRT5* locus. The two upper tracks show normalized enrichment of endogenous (BxPC3) or overexpressed (ΔNp63-FLAG SUIT2) ΔNp63. The bottom four tracks show H3K27ac normalized enrichment after GFP or ΔNp63 overexpression in SUIT2 cells or *ROSA26* or *TP63* knockout in BxPC3 cells. ChIP signal was calculated using deepTools with the option BamCompare subtract to normalize each sample to its input. All tracks plotting ChIP data obtained with the same antibody are plotted in the same scale. **c**–**e**, Western blot of basal-like markers in *TP63* or *MED12* knockout human patient-derived basal-like PDAC organoid hF3 (**c**), HNSCC (Cal33), SSCC (Hsc5), basal-like TNBC (HCC1806) and ESCC (KYSE70 and KYSE410) human cancer cell lines (**d**), and patient-derived TNBC organoid NH93T (**e**). HNSCC: head and neck squamous cell carcinoma; SSCC: skin squamous cell carcinoma; TNBC: triple-negative breast cancer; ESCC: esophageal squamous cell carcinoma.
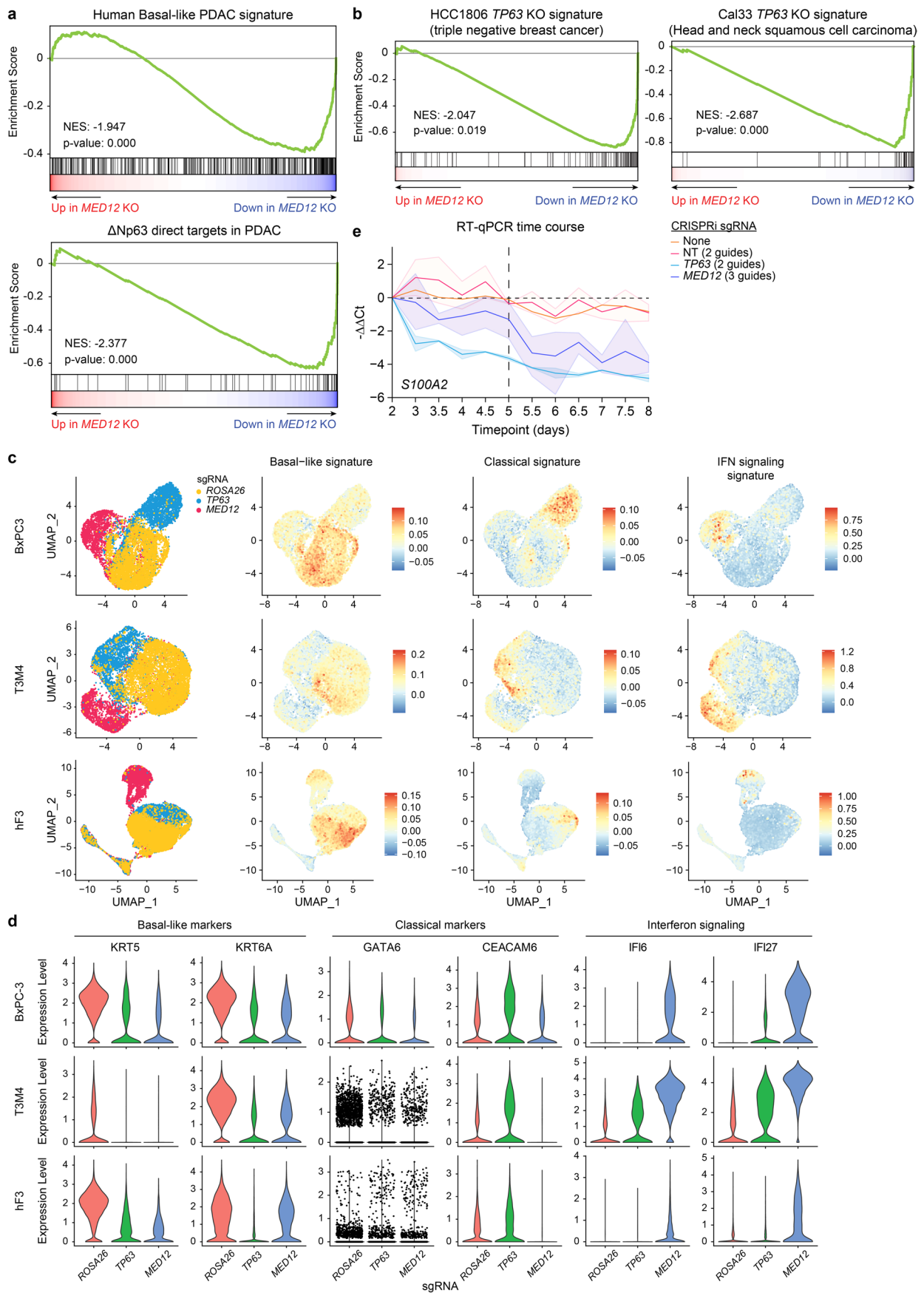
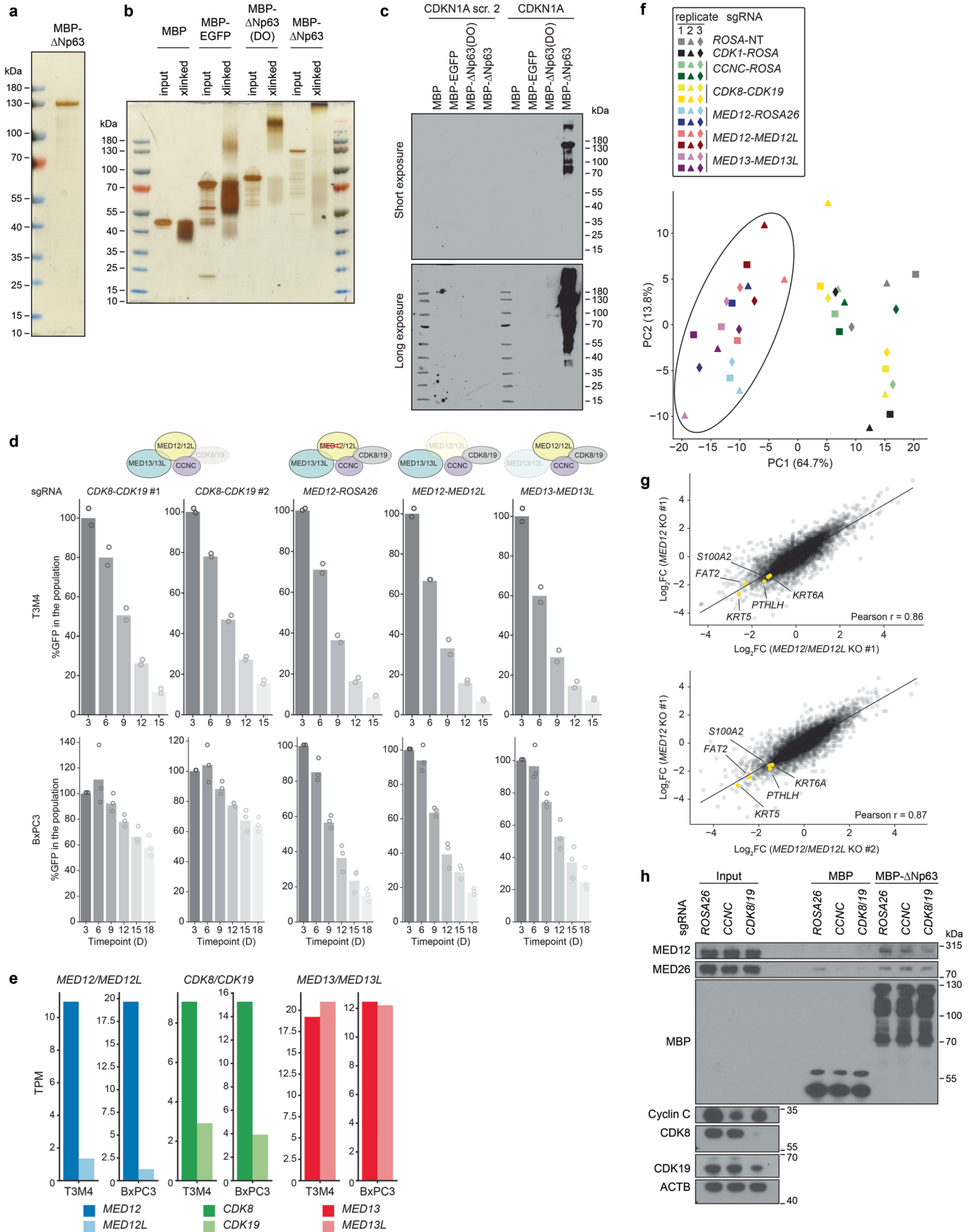**Extended Data Fig. 2 | See next page for caption.**

Extended Data Fig. 2 | MED12 and ΔNp63 co-regulate the basal gene expression program. a, Representative GSEA plots of KLM1 *MED12* knockout using gene signatures derived from human basal PDAC tumors[10] and direct ΔNp63 gene targets in PDAC[18]. Three biological replicates were used for each sample. Complete GSEA analysis for all the sgRNA and cell lines tested can be found in Supplementary Table 3. **b**, Representative GSEA plots of HCC1806 (basal-like TNBC) and Cal33 (HNSCC) *MED12* knockout using ΔNp63 target gene signatures. Two biological replicates were used for each sample, and two different sgRNAs were tested per gene. Complete GSEA analysis for all the sgRNA tested can be found in Supplementary Table 4. **c**, UMAPs of BxPC3 (top row), T3M4 (middle row) and hF3 (bottom row) scRNA-seq upon CRISPR knockout of *TP63* or *MED12*. Each unique cell sequenced is colored according to its knockout genotype on the leftmost column to illustrate the distribution of cells in the UMAP. UMAP heatmaps colored by intensity of basal-like PDAC[18], classical PDAC[10] and Interferon alpha/beta (MSigDB R-HSA-909733 v2023.1) signatures are shown

on the right. Pre-processing and data filtering were performed as described in Methods. **d**, Violin plots of gene expression of basal-like marker genes *KRT5* and *KRT6A*, classical genes *GATA6* and *CEACAM6* and Interferon-related genes *IFI6* and *IFI27* across BxPC3, T3M4 and hF3 knockout scRNA-seq. When density of cells expressing non-negligible levels of assessed genes was low across all conditions, individual cell expression values were depicted as single dots. **e**, Time-course RT-qPCR of *S100A2* after lentiviral infection with CRISPRi sgRNA targeting *TP63* (2 sgRNA), *MED12* (3 sgRNA), non-targeting sgRNAs (2 sgRNA) or uninfected control T3M4 cells. −ΔΔCt values are plotted as the average of each sgRNA normalized to the average of housekeeping genes *ACTB* and *B2M* (three measurements per condition). For each gene perturbation, the average −ΔΔCt value is shown in a solid line, and the 95% confidence intervals are shown as translucid intervals. The inflection points of *TP63* and other basal markers upon *MED12* knockdown (~day 5) is marked by a vertical black dashed line.
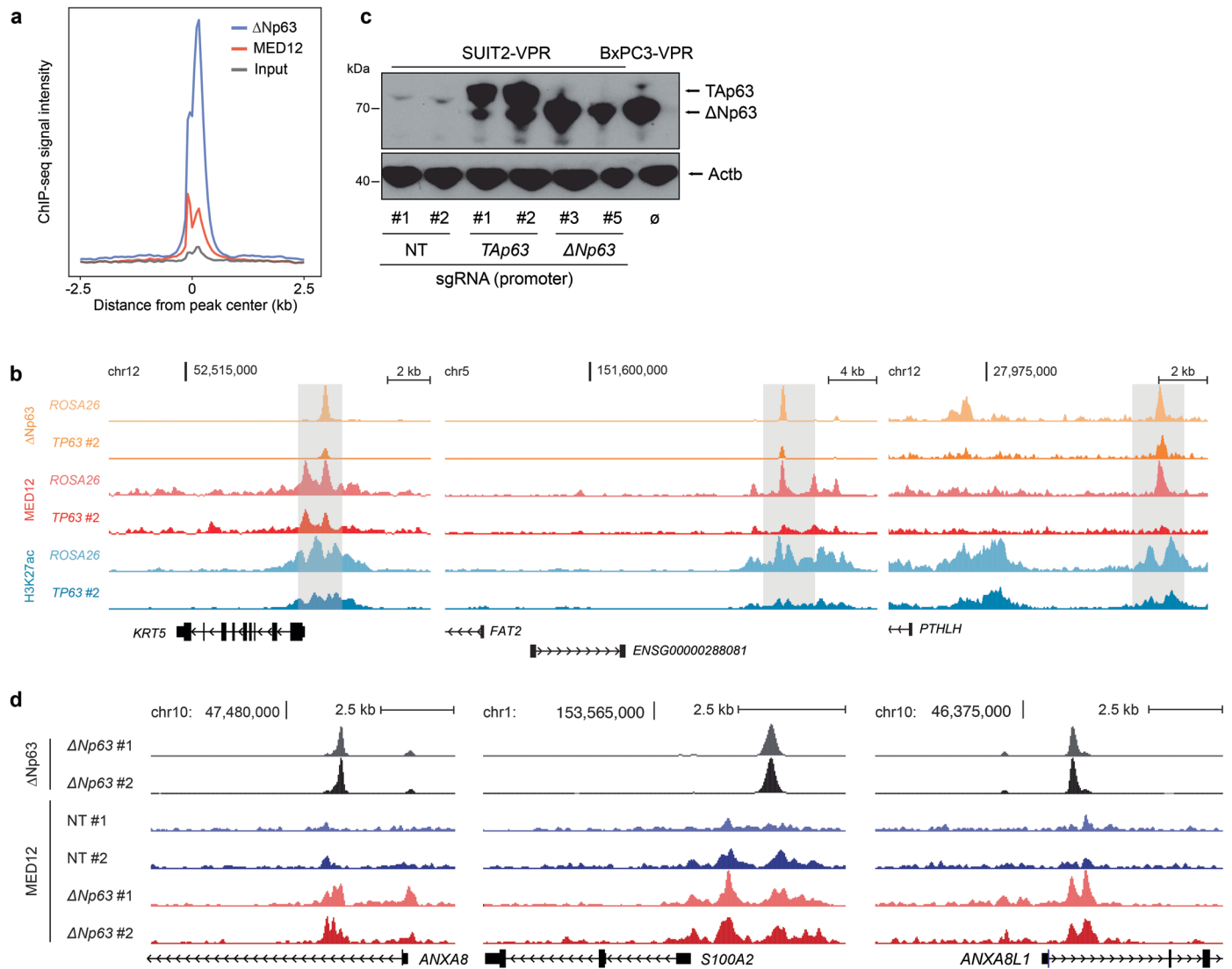
Extended Data Fig. 3 | MED12 and ΔNp63 co-occupy basal-like loci. a, Metaplot of genomic occupancy of ΔNp63 and MED12 centered around ΔNp63 peaks in T3M4 cells. **b**, ChIP−seq tracks of ΔNp63, MED12 and H3K27ac normalized occupancy at select basal-specific ΔNp63 direct target loci in KLM1 cells upon *ROSA26* or *TP63* knockout (sgRNA, 2). Normalized enrichment values were generated with deepTools bamCoverage -RPCG. **c**, Western blot of SUIT2 CRISPR-activated *TP63* (*ΔNp63* isoform-specific) cells. BxPC3, which endogenously expresses the ΔN isoform of p63, is shown as a positive control in the rightmost lane. **d**, Genomic tracks of ΔNp63 and MED12 occupancy at direct ΔNp63 targets *ANXA8*, *S100A2* and *ANXA8L1* in SUIT2-VPR lines infected with non-targeting (NT) or *TP63*-targeting sgRNAs. **a,b,d**, One independent measurement is shown per condition.

Extended Data Fig. 4 | See next page for caption.

Extended Data Fig. 4 | Characterization of recombinantly expressed and purified full length MBP-p63 protein and MKM-dependent association of ΔNp63 with Mediator. a, Silver stain of full length purified MBP-ΔNp63. The single protein band was confirmed to be the expected MBP-ΔNp63 peptide by western blotting and mass spectrometry. **b**, Silver stain of 0.025% glutaraldehyde crosslinked ('xlinked') and input purified full length MBP-ΔNp63, MBP-ΔNp63 truncation mutant (DO, DBD through OD), MBP-EGFP or MBP alone. **c**, Western blot of DNA pulldown experiment using purified proteins and biotinylated DNA oligos containing the p63-binding sequence of the *CDKN1A* promoter or a scramble DNA control. **d**, Competition-based proliferation assays in Cas9-expressing T3M4 (top row) and BxPC3 (bottom row) cells after lentiviral expression of the indicated sgRNA pairs linked with GFP. Bars represent the mean normalized percentage of GFP to day 3 after infection, and dots represent independent measurements (n=3 biological replicates). **e**, Transcripts per million gene expression levels of paralog pairs of the MKM in T3M4 and BxPC3 cell lines. Data extracted from the CCLE dataset. **f**, Principal component analysis of gene expression changes upon MKM paralog double knockout. *MED12*, *MED12/MED12L* and *MED13/MED13L* double knockouts are encircled together. **g**, Scatterplots depicting gene expression changes in *MED12* or *MED12/MED12L* knockout T3M4 cells. DESeq2-derived log$_2$(FC) of all significantly expressed genes in three biological replicates per sgRNA are plotted. Select basal genes are highlighted in yellow. **h**, Western blot of MBP or MBP-ΔNp63 pulldown of endogenous Mediator components from nuclear lysates of *ROSA26*, *CCNC* or *CDK8/CDK19* knockout HEK293T cells.
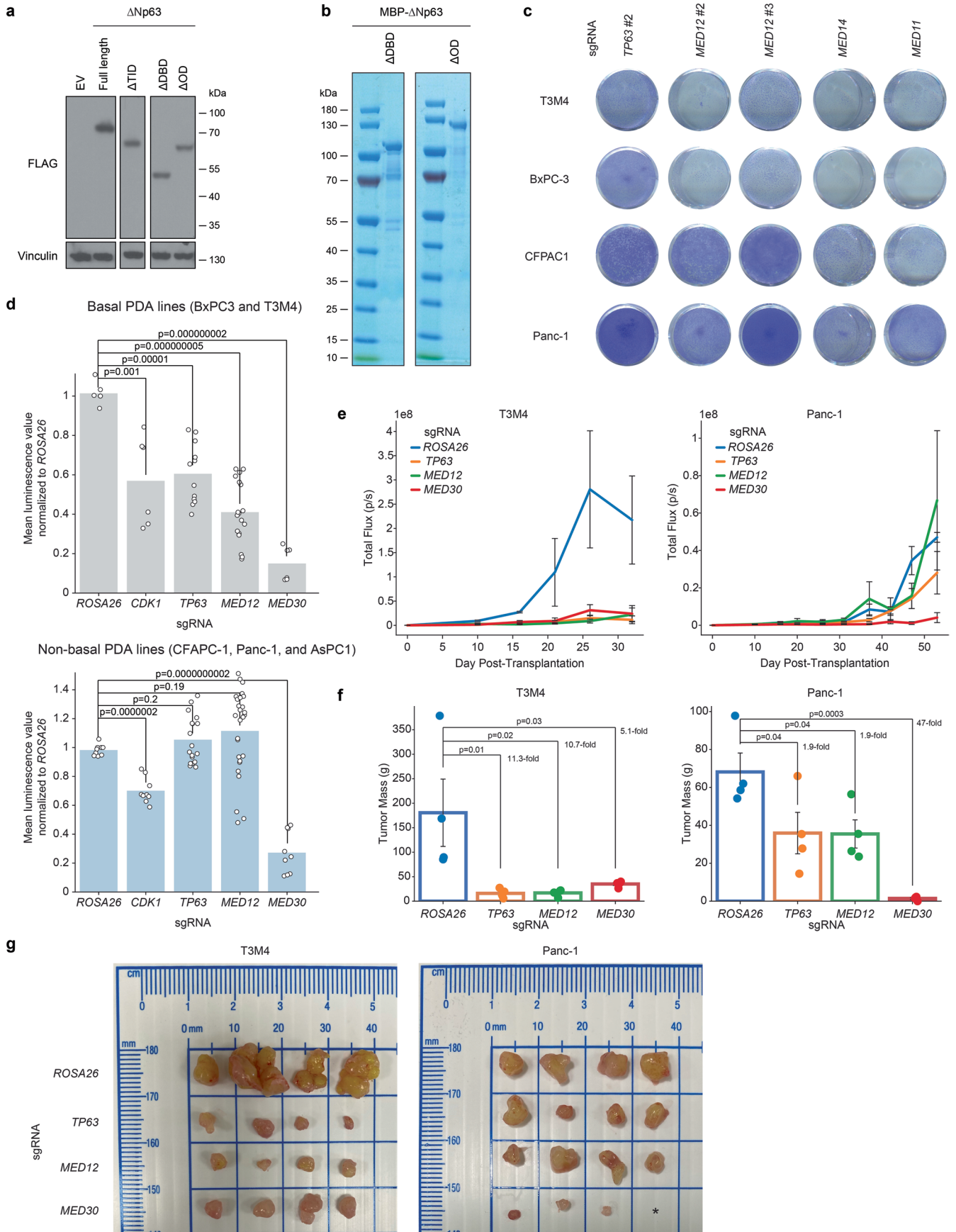
Extended Data Fig. 5 | See next page for caption.

Extended Data Fig. 5 | *MED12* is a preferential genetic dependency in basal-like PDAC. a, Western blots of T3M4 cells stably expressing N-FLAG-tagged overexpressed truncated ΔNp63 cDNA used in gene complementation assays in Fig. 4b. **b**, Coomassie blue of purified MBP-ΔNp63 mutants lacking the DNA-binding domain (ΔDBD) or oligomerization domain (ΔOD). **c**, Crystal violet staining of basal-like (T3M4, BxPC3) or classical (CFPAC1, Panc-1) knockout cell lines of *TP63*, *MED12*, or pan-essential core Mediator subunits *MED11* and *MED14*. **d**, Luminescence reading of CellTiter-Glo assay at day 8 post-infection with lentivirally-encoded sgRNA (n=2–3 independent replicates). Two-sided t-test p-values are shown in the figure. **e**, Orthotopically transplanted basal-like ΔNp63+ (T3M4) or ΔNp63- (Panc-1) knockout cells were followed over time by luciferase imaging (n=4 mice per group per cell line). Growth of *TP63* and *MED12* knockout tumor cells was compared with that of negative control (*ROSA26*

targeting sgRNA) and core Mediator (pan-essential *MED30*) knockout. Average of independent sample measurements is shown per timepoint, with error bars depicting the standard error of the mean. **f**, Resected tumor weight at endpoint in T3M4 and Panc-1 knockout cells (n=4 mice per group per cell line). Independent tumor samples are shown as dots, and their average value is shown as bars along with error bars depicting the standard error of the mean. The fold decrease in tumor mass compared to *ROSA26* knockout is shown next to the bar of each additional knockout condition. A one-way ANOVA was conducted to detect any overall differences among the groups, followed by Dunnett's test to compare each sgRNA knockout against the *ROSA26* knockout control. *P*-values are displayed to indicate the significance of these comparisons. **g**, Images of resected of T3M4 and Panc-1 orthotopic tumors. An asterisk indicates that despite initial injection of tumor cells, no tumor mass could be found at endpoint.
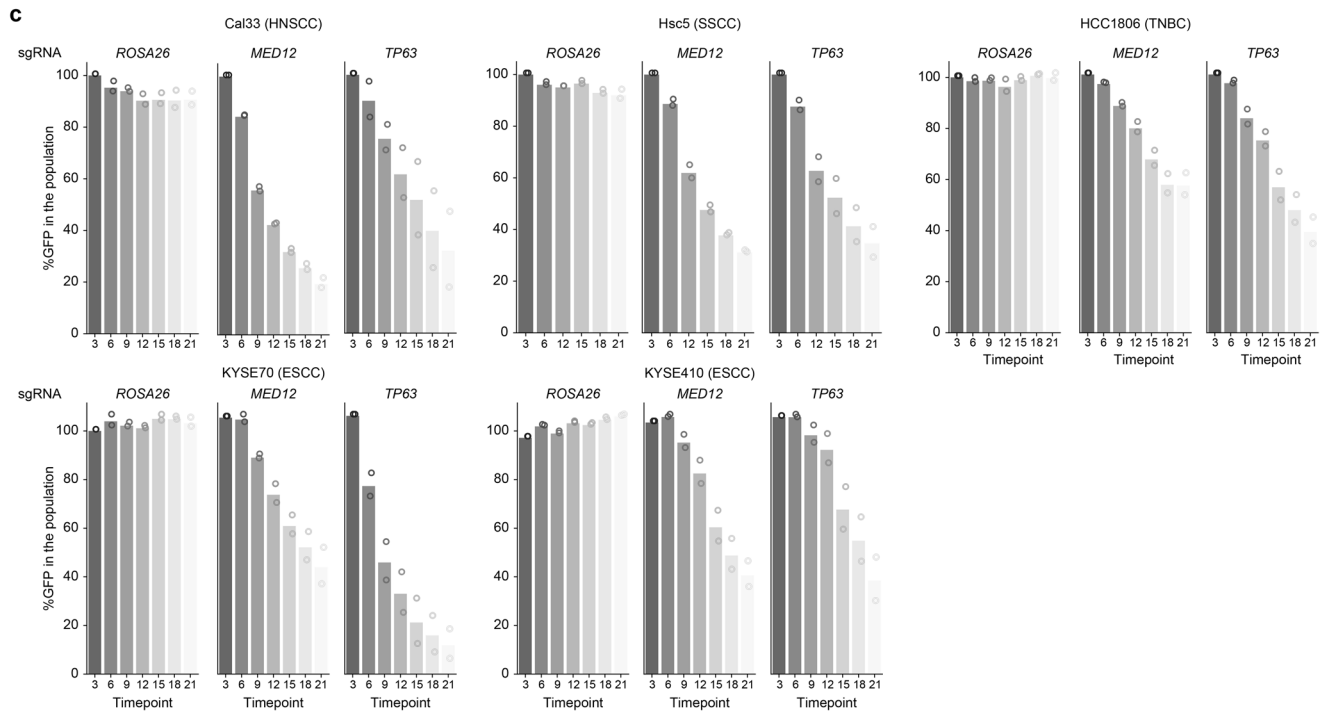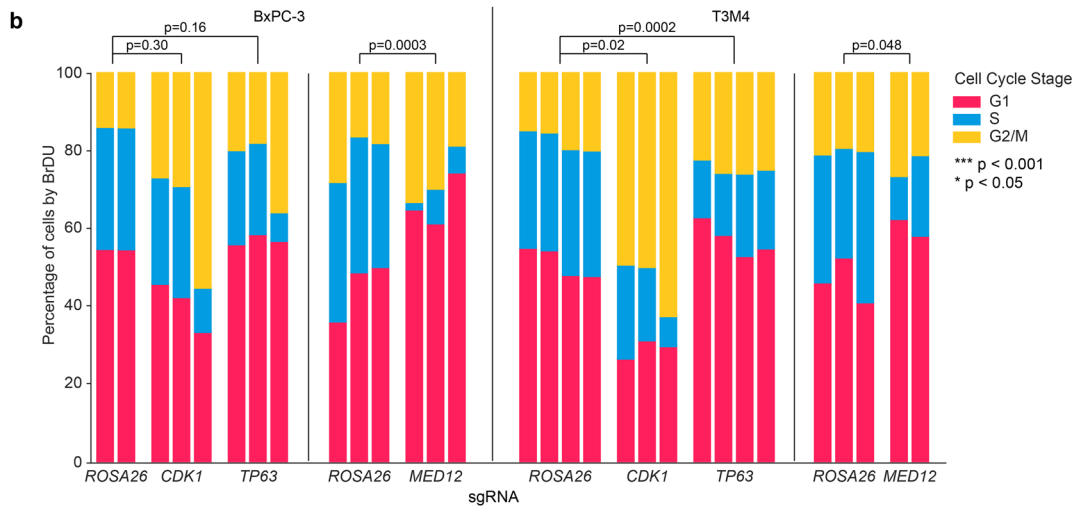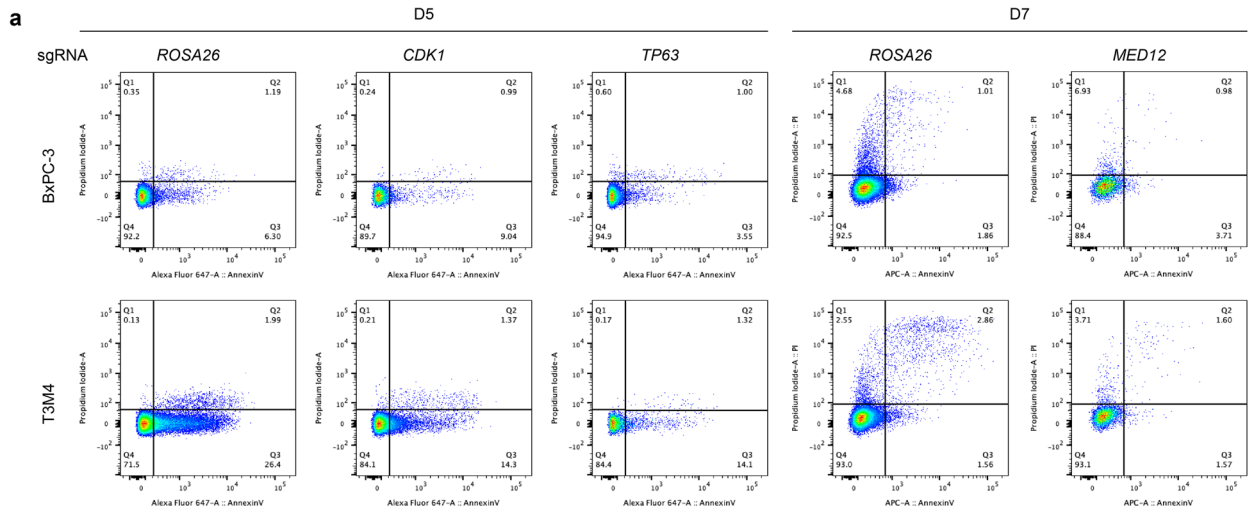
Extended Data Fig. 6 | See next page for caption.

Extended Data Fig. 6 | Flow cytometry-based cell cycle profiling reveals growth arrest in *TP63* and *MED12* knockout cells. a, Flow cytometry plots of BxPC3 (top) or T3M4 (bottom) knockout cells stained with propidium iodide (y-axis) and AF647-Annexin V (x-axis). Events shown were previously gated on singlets by FSC-H vs FSC-W. Percentages of events relative to the total number of gated events is shown in each quadrant. **b**, Stacked bar plot representing the distribution of singlets in each cell cycle phase by BrdU staining in BxPC3 (left) or T3M4 (right) knockout cells. Each stacked bar represents the distribution of events for an independent measurement. Two-sided t-test p-value of proportion of cells in S phase are shown in the figure. **c**, Competition-based proliferation assays in Cas9-expressing Cal33 (HNSCC), Hsc5 (SSCC), HCC1806 (TNBC), KYSE70 (ESCC) and KYSE410 (ESCC) after lentiviral expression of *TP63*- or *MED12*-targeting sgRNAs. Bars represent the mean percentage GFP normalized to day 3 post-infection, and dots represent independent measurements (n=2 biological replicates). HNSCC: head and neck squamous cell carcinoma; SSCC: skin squamous cell carcinoma; TNBC: triple-negative breast cancer; ESCC: esophageal squamous cell carcinoma.

Corresponding author(s): Christopher Vakoc

Last updated by author(s): Mar 22, 2024

Reporting Summary

Nature Portfolio wishes to improve the reproducibility of the work that we publish. This form provides structure for consistency and transparency in reporting. For further information on Nature Portfolio policies, see our Editorial Policies and the Editorial Policy Checklist.

Statistics

For all statistical analyses, confirm that the following items are present in the figure legend, table legend, main text, or Methods section.

n/a	Confirmed	
☐	☒	The exact sample size (*n*) for each experimental group/condition, given as a discrete number and unit of measurement
☐	☒	A statement on whether measurements were taken from distinct samples or whether the same sample was measured repeatedly
☐	☒	The statistical test(s) used AND whether they are one- or two-sided
		Only common tests should be described solely by name; describe more complex techniques in the Methods section.
☒	☐	A description of all covariates tested
☒	☐	A description of any assumptions or corrections, such as tests of normality and adjustment for multiple comparisons
☐	☒	A full description of the statistical parameters including central tendency (e.g. means) or other basic estimates (e.g. regression coefficient) AND variation (e.g. standard deviation) or associated estimates of uncertainty (e.g. confidence intervals)
☐	☒	For null hypothesis testing, the test statistic (e.g. *F*, *t*, *r*) with confidence intervals, effect sizes, degrees of freedom and *P* value noted
		Give P values as exact values whenever suitable.
☒	☐	For Bayesian analysis, information on the choice of priors and Markov chain Monte Carlo settings
☒	☐	For hierarchical and complex designs, identification of the appropriate level for tests and full reporting of outcomes
☐	☒	Estimates of effect sizes (e.g. Cohen's *d*, Pearson's *r*), indicating how they were calculated

Our web collection on statistics for biologists contains articles on many of the points above.

Software and code

Policy information about availability of computer code

Data collection	MACSQuant Analyzer was used to acquire and analyze flow cytometry data for GFP competitions and gene complementation assays. QuantStudio 6 Flex System (Applied Biosystems) was used to acquire RT-qPCR data. SoftMax Pro V6.3 (moleculardevices.com) was used to measure luminescence and OD570.
Data analysis	Python (3.6.0) was used for data analysis. Seurat (4.3.0.1) was used for scRNA-seq analysis. Bowtie2(2.3.5.1), Samtools (1.11), Macs2 (2.2.6), Bedtools (2.30.0), Homer (v4.11), and deepTools (3.5.0) were used for ChIP-Seq analysis. STAR (2.7.9a), HTSeq-count (2.21), DESeq2 (1.38.0) were used for RNA-Seq analysis. MAGeCK (0.5.9.3) was used for CRISPR screens analysis. GSEApy (1.0.0) was used for Gene Set Enrichment Analysis. Visualization of ChIP-Seq profile was done on UCSC genome browser. Scipy was used to perform statistical analysis. Cell Flow cytometry analysis was performed with FlowJo software (V10.6.2).

For manuscripts utilizing custom algorithms or software that are central to the research but not yet described in published literature, software must be made available to editors and reviewers. We strongly encourage code deposition in a community repository (e.g. GitHub). See the Nature Portfolio guidelines for submitting code & software for further information.

Data

Policy information about availability of data

All manuscripts must include a data availability statement. This statement should provide the following information, where applicable:
- Accession codes, unique identifiers, or web links for publicly available datasets
- A description of any restrictions on data availability
- For clinical datasets or third party data, please ensure that the statement adheres to our policy

> All RNA-seq, scRNA-seq, ChIP-Seq and CRISPR screening data generated from this study is available through Gene Expression Omnibus (GEO) database. The accession number is GSE229062. Hg38 human genome (UCSC) was used for all analyses.

Research involving human participants, their data, or biological material

Policy information about studies with human participants or human data. See also policy information about [sex, gender (identity/presentation), and sexual orientation](sex, gender) and race, ethnicity and racism.

Reporting on sex and gender	N/A.
Reporting on race, ethnicity, or other socially relevant groupings	N/A.
Population characteristics	N/A.
Recruitment	N/A.
Ethics oversight	N/A.

Note that full information on the approval of the study protocol must also be provided in the manuscript.

Field-specific reporting

Please select the one below that is the best fit for your research. If you are not sure, read the appropriate sections before making your selection.

☒ Life sciences   ☐ Behavioural & social sciences   ☐ Ecological, evolutionary & environmental sciences

For a reference copy of the document with all sections, see nature.com/documents/nr-reporting-summary-flat.pdf

Life sciences study design

All studies must disclose on these points even when the disclosure is negative.

Sample size	No statistical method was used to calculate sample size and sample sizes were deemed appropriate for each experiment according to expected effect sizes. All sample sizes were determined to be sufficient given that the differences among groups were consistent.
Data exclusions	No data was excluded.
Replication	The reported results were replicated across multiple experiments to generated reliable results and are described in more detail in the figure legends and methods section.
Randomization	Randomization was not required in our experimental designs and thus not performed for any experiment.
Blinding	Blinding was not possible in our experimental designs and thus not performed for any experiment.

Reporting for specific materials, systems and methods

We require information from authors about some types of materials, experimental systems and methods used in many studies. Here, indicate whether each material, system or method listed is relevant to your study. If you are not sure if a list item applies to your research, read the appropriate section before selecting a response.

Materials & experimental systems

n/a	Involved in the study
☐	☒ Antibodies
☐	☒ Eukaryotic cell lines
☒	☐ Palaeontology and archaeology
☐	☒ Animals and other organisms
☒	☐ Clinical data
☒	☐ Dual use research of concern
☒	☐ Plants

Methods

n/a	Involved in the study
☐	☒ ChIP-seq
☐	☒ Flow cytometry
☒	☐ MRI-based neuroimaging

Antibodies

Antibodies used	All antibodies used in this study are the following: p63α (Cell Signaling D2K8X), Keratin 5 (Cell Signaling D4U8Q), MED12 (Cell Signaling D9K5J), CDK8 (Cell Signaling D6M3J), CCNC (Cell Signaling E6V4Z), MED1 (Bethyl Laboratories A300-793A), MED13L (Bethyl Laboratories A302-421A), MED15 (Bethyl Laboratories A302-422A), MED16 (Bethyl Laboratories A303-668A), MED23 (Invitrogen PA5-37444), MED24 (Bethyl Laboratories A301-472A), MED25 (Invitrogen PA5-43617), MED26 (Cell Signaling D4B1X), MED30 (ProteinTech PTG 16787-1-AP), H3K27ac (Abcam ab4729), FLAG (Sigma F3165), MBP (NEB E8032), HA-HRP (Roche 12013819001), Alexa Fluor 647-conjugated goat anti-rabbit (Invitrogen A-21245). For western blot, the following items and dilutions were used: p63α (1:1000), Keratin 5 (1:1000), MED12 (1:1000), CDK8 (1:1000), CCNC (1:500), MED1 (1:2000), MED13L (1:1000), MED15 (1:1000), MED16 (1:1000), MED23 (1:500), MED24 (1:1000), MED25 (1:500), MED26 (1:1000), MED30 (1:500), FLAG (1:5000), MBP (1:5000), and HA-HRP (1:5000). For ChIP-seq, the following items and dilutions were used: p63α (5µL/IP), MED12 (10µL/IP), and H3K27ac (4µg/IP). For flow cytometry, the following items and dilutions were used: p63α (1:400), Keratin 5 (1:400), and Alexa Fluor 647-conjugated goat anti-rabbit (1:500).
Validation	p63α (D2K8X, Cell Signaling) and KRT5 (D4U8Q, Cell Signaling) antibodies were validated through CRISPRa overexpression, CRISPR knockout, and CRISPRi knockdown of TP63 in human PDAC cell lines and detection of the correct product via western blot or flow cytometry intensity values. MED12 (D9K5J, Cell Signaling) antibody was validated through knockout in different cell lines and presence in mass spectrometry-validated partially purified Mediator. p63α (D2K8X, Cell Signaling), MED12 (D9K5J, Cell Signaling), and CDK8-kinase module antibodies were further validated through purified or partially purified reconstituted preparations followed by western blot. Other human Mediator antibodies were validated through cDNA overexpression in Sf9 cells, which specifically acquired signal exclusively upon matching cDNA overexpression. FLAG (F3165, Sigma), MBP (E8032, NEB), and HA-HRP (12013819001, Roche) were validated by the vendors for human cell use and by us through immunoprecipitation assays using tagged overexpressed proteins of known size in human cancer cell lines.

Eukaryotic cell lines

Policy information about cell lines and Sex and Gender in Research

Cell line source(s)	The following cell lines used in this study were obtained from ATCC: PANC1 (Cat# CRL-1469, RRID:CVCL_0480), CFPAC1 (Cat# CRL-1918, RRID:CVCL_1119), AsPC1 (CRL-1682, RRID:CVCL_0152), MIAPaca2 (Cat# CRL-1420, RRID:CVCL_0428), and BxPC3 (Cat# CRL-1687, RRID:CVCL_0186). The following cell lines used in this study were obtained from JCRB: SUIT2 (JCRB1094, RRID:CVCL_3172), T3M4 (RCB1021, RRID:CVCL_4056), KLM1 (RCB2138, RRID:CVCL_5146), and PK-1 (RCB1972, RRID:CVCL_4717). HeLa cell line was a gift from Bruce Stillman's lab at Cold Spring Harbor Laboratory and Sf9 cell line was a gift from Leemor Joshua-Tor's lab at Cold Spring Harbor Laboratory.
Authentication	Cell lines were validated by the vendor (ATCC) using STR profiling and cell morphology analysis. Cell lines were further validated by STR profiling at an external facility after the establishment of Cas9 stable cell lines (Genetics core, University of Arizona). We verified that all human pancreatic cancer lines used in our study demonstrated the correct cell morphology throughout our studies, with BxPC-3, KLM1, and T3M4 displaying characteristic growth in adherent cell nests.
Mycoplasma contamination	All cell lines are regularly verified to be mycoplasma contamination free.
Commonly misidentified lines (See ICLAC register)	No ICLAC cell lines were used.

Animals and other research organisms

Policy information about studies involving animals; ARRIVE guidelines recommended for reporting animal research, and Sex and Gender in Research

Laboratory animals	Mus musculus NSG (NOD.Cg-Prkdc scid Il2rg tm1Wjl /SzJ), 6 weeks, #005557, The Jackson Laboratory. Experiments were done in 8-

Laboratory animals	to 10-week animals. Mice were kept in standard animal husbandry conditions according to Cold Spring Harbor Laboratory animal handling guidelines.
Wild animals	No wild animals were used in this study.
Reporting on sex	All NSG mice used were female.
Field-collected samples	No field collected samples were used in this study.
Ethics oversight	Experimental protocols involving mice were approved by the institutional animal care and use committees (IACUC) at Cold Spring Harbor Laboratory.

Note that full information on the approval of the study protocol must also be provided in the manuscript.

Plants

Seed stocks	N/A.
Novel plant genotypes	N/A.
Authentication	N/A.

ChIP-seq

Data deposition

☒ Confirm that both raw and final processed data have been deposited in a public database such as GEO.

☒ Confirm that you have deposited or provided access to graph files (e.g. BED files) for the called peaks.

Data access links *May remain private before publication.*	All ChIP-Seq data generated from this study is available through Gene Expression Omnibus (GEO) database. The accession number is GSE229062.
Files in database submission	Fastq files and bigWig output from DeepTools BamCoverage: klm1-parental-input klm1-parental-chip-med12 klm1-parental-chip-p63 t3m4-parental-input t3m4-parental-chip-med12 t3m4-parental-chip-p63 klm1-ko-rosa26-chip-h3k27ac klm1-ko-rosa26-chip-med12 klm1-ko-rosa26-chip-p63 klm1-ko-rosa26-input-chip-med12 klm1-ko-rosa26-input-chip-p63_h3k27ac klm1-ko-tp63-1-chip-h3k27ac klm1-ko-tp63-1-chip-med12 klm1-ko-tp63-1-chip-p63 klm1-ko-tp63-1-input-chip-med12 klm1-ko-tp63-1-input-chip-p63_h3k27ac klm1-ko-tp63-2-chip-med12 klm1-ko-tp63-2-chip-p63 klm1-ko-tp63-2-chip-h3k27ac klm1-ko-tp63-2-input-chip-med12 klm1-ko-tp63-2-input-chip-p63_h3k27ac SUIT2-DELTAN-3-input SUIT2-DELTAN-3-chip-MED12 SUIT2-DELTAN-3-chip-P63 SUIT2-DELTAN-5-input SUIT2-DELTAN-5-chip-MED12 SUIT2-DELTAN-5-chip-P63 SUIT2-NEG-1-input SUIT2-NEG-1-chip-MED12 SUIT2-NEG-2-input SUIT2-NEG-2-chip-MED12
Genome browser session (e.g. UCSC)	https://genome.ucsc.edu/s/diogomaiasilva/maiasilva23

Methodology

Replicates	For p63 and MED12 ChIP-seq in parental T3M4 and KLM1, KLM1 KO, and SUIT2 CRISPRa ChIP-seq, one replicate of each sgRNA tested was done.
Sequencing depth	40-60 million single-end reads were sequenced for each sample.
Antibodies	For ChIP-seq, the following antibodies were used: p63α (D2K8X, Cell Signaling), MED12 (D9K5J, Cell Signaling), and H3K27ac (ab4729, Abcam).
Peak calling parameters	Mappability of each sample was higher than 70%. For narrow peak (p63 and MED12) and broad peak (H3K27ac) calling, MACS2 default parameters were used.
Data quality	Only peaks nominated with FDR 5% by MACS2 were used in this study.
Software	Sequencing reads were mapped to the hg38 genome using Bowtie2 v2.3.5.1 with default settings. MACS v2.2.6 was used to call peaks using input genomic DNA as control. Annotation of ChIP-seq peaks was performed using HOMER v4.11 with default settings. To visualize genomic tracks, bigWig files were generated from BAM files using deepTools v3.5.0 bamCoverage function normalizing with reads per genome coverage. To define BED files of peaks and peak overlaps, MACS2 output narrowPeak or broadPeak files were merged using bedtools v2.30.0 merge and intersect tools. Heatmaps and average chromatin occupancy metaplots were generated using computeMatrix and plotHeatmap functions of deepTools, taking bigWig files and BED files as input.

Flow Cytometry

Plots

Confirm that:

☒ The axis labels state the marker and fluorochrome used (e.g. CD4-FITC).

☒ The axis scales are clearly visible. Include numbers along axes only for bottom left plot of group (a 'group' is an analysis of identical markers).

☒ All plots are contour plots with outliers or pseudocolor plots.

☒ A numerical value for number of cells or percentage (with statistics) is provided.

Methodology

Sample preparation	Cas9-, dCas9-KRAB-, or dCas9-VPR-expressing pancreatic cancer cell lines (KLM1, BxPC3, T3M4) were infected with lentiviral individual sgRNA or pooled CRISPR libraries and fixed in 100% -20C methanol at endpoint. After a minimum of 6h, cells were washed 1x in FACS buffer (1% (w/v) ultrapure BSA, 0.5% (w/v) sodium azide, and 1mM EDTA in magnesium and calcium-free PBS) and stained with primary antibody overnight rotating at 4C. After 2x washes, incubation with secondary antibody for 1/2h, and 2x washes, samples were acquired in the following hour.
Instrument	LSR Dual Fortessa flow cytometer (BD Biosciences) was used for FACS. FACS Aria sorter (BD Biosciences) was used for flow cytometry-assisted cell sorting with the laser 633nm.
Software	FlowJo (Version 10, BD Biosciences) was used for FACS data analysis.
Cell population abundance	Cell populations sorted by protein abundance were subsequently subjected to DNA extraction and library preparation.
Gating strategy	For flow cytometry-based CRISPR screens, side scatter area (SSC-A) plot vs forward scatter (FSC-A) area was used to separate live cells from debris and dead cells. The SSC height versus width and FSC height versus width were sequentially gated to separate single cells from aggregates. The highest 15% and bottom 30% percentiles of AF647 signal (elicited with 633nm laser) were sorted into marker high and marker low pools.

☒ Tick this box to confirm that a figure exemplifying the gating strategy is provided in the Supplementary Information.